TAMPEREEN TEKNILLINEN YLIOPISTO
TAMPERE UNIVERSITY OF TECHNOLOGY

**HUSSAIN SHABAN A. Ali**

# POWER ALLOCATION IN CARRIER AGGREGATION MIMO SYSTEMS WITH DIFFERENT POWER CONSTRAINTS

Master of Science Thesis

Examiners: Professor Mikko Valkama
and Professor Markku Renfors
Examiners and topic approved in the Faculty of Computing and Electrical Engineering Council meeting on 3rd April 2013

# ABSTRACT

**TAMPERE UNIVERSITY OF TECHNOLOGY**
Master's Degree Program in Information Technology
**Ali, Hussain Shaban A.:** Power Allocation in Carrier Aggregation MIMO Systems with Different Power Constraints
Master of Science Thesis: 48 Pages, 3 Appendix Pages
August 2013
Major: Communications Engineering
Examiners: Professor Mikko Valkama and Professor Markku Renfors
Keywords: BER Performance, Carrier Aggregation, CA-MIMO, LTE-Advanced, Modified Hybrid Gradient, Optimal Power Allocation, Power Control

The target set by the International Telecommunication Union (ITU) for the next generation of mobile communications, IMT-Advanced, is to achieve up to 1 Gb/s peak data rates. The 3rd Generation Partnership Project (3GPP) introduced Carrier Aggregation (CA) technology in its latest Long Term Evolution Advanced (LTE-Advanced) standards in order to meet the performance goals of the next generation, the fourth generation, 4G.

The introduction of CA in LTE-Advanced system poses a challenge to the power control function of a CA-MIMO radio link. The problem appears when multiple Carrier Components (CCs), within a single or multiple frequency bands, are allocated to a user. The two challenges studied in this thesis are the different channel characteristics in the different CCs and the multiple power constraints imposed on the mobile equipment: per-CC, per-antenna and per-total transmit power available. This thesis studies the bit error rate (BER) performance of a CA-MIMO radio link with the Modified Hybrid Gradient Optimal Power Allocation (MHGOPA) algorithm. In order to examine the validity of the MHGOPA algorithm, the results are compared to a baseline uniform power allocation approach.

The results of the simulations are obtained for different environments: Indoor Hotspot, Urban Microcell, Suburban Microcell and Urban Macrocell. The results show that the MHGOPA algorithm generally outperforms the baseline uniform power allocation when the channel conditions are good with typical SNR values above 8-10 dB, depending on the environment. The results also show a marginal improvement on the BER in some scenarios when relaxing the constraints on the antennas. The simulations also show that giving primary carrier components (PCC) a privilege in power results in a large degradation in overall performance.

# PREFACE

This Master of Science Thesis work, "Power Allocation in Carrier Aggregation MIMO Systems with Different Power Constraints," has been written for the completion of my M.Sc degree in Tampere University of Technology, Department of Electronics and Communications Engineering.

I would like first to thank my supervisor Prof. Mikko Valkama for introducing me to the thesis topic and for the advice and guidance he provided during my thesis work. I would also like to give my thanks for Prof. Markku Renfors for his comments and help to improve my thesis work.

Additionally, I am very grateful for all the support I got from my parents and family during my years while studying in Finland. With their support and encouragement, I am able to be where I am now.

Tampere, 19th August 2013

Hussain Shaban A. Ali

## Contents

# LIST OF ABBREVIATIONS

| | |
|---|---|
| 1G | First Generation |
| 2G | Second Generation |
| 3G | Third Generation |
| 3GPP | Third Generation Partnership Project |
| 4G | Fourth Generation |
| ADV | Advanced |
| AMPS | Advanced Mobile Phone System |
| AoA | Angle of Arrival |
| AoD | Angle of Departure |
| AS | Angle Spread |
| ASA | AoA Spread |
| ASD | AoD Spread |
| BER | Bit Error Rate |
| BS | Base Station |
| BTS | Base Transceiver Station |
| BW | Bandwidth |
| CA | Carrier Aggregation |
| CC | Carrier Component |
| CDL | Clustered Delay Line |
| CDMA | Code Division Multiple Access |
| CGM | Conjugate Gradient Method |
| CSI | Channel State Information |
| DAC | Digital to Analog Converter |
| DFTS-FDMA | Discrete Fourier Transform Spread- Frequency Division Multiple Access |
| DL | Downlink |
| DS | Delay Spread |
| EDGE | Enhanced Data Rates for GSM Evolution |
| eNode B | Evolved Node B |
| EPC | Evolved Packet Core |
| EPS | Evolved Packet System |
| E-UTRAN | Evolved Universal Terrestrial Radio Access |
| FEM | Finite Element Method |
| FFT | Fast Fourier Transform |
| FRS | Fixed Relay Station |
| GPM | Gradient Projection Method |
| GPRS | General Packet Radio Service |
| GSM | Global System for Mobile Communications |
| HF | High Frequency |
| HSDPA | High Speed Downlink Packet Access |
| HSPA | High Speed Packet Access |
| HSPA+ | Evolved High Speed Packet Access |
| HSUPA | High Speed Uplink Packet Access |
| IEEE | Institute of Electrical and Electronics Engineers |
| IF | Intermediate Frequency |

| | |
|---|---|
| IFFT | Inverse Fast Fourier Transform |
| IMT | International Mobile Telecommunication |
| InH | Indoor Hotspot |
| IP | Internet Protocol |
| ITU | International Telecommunication Union |
| ITU-R | ITU Radio-communication Sector |
| LOS | Line of Sight |
| LS | Large Scale |
| LTE | Long Term Evolution |
| MAC | Media Access Control |
| ME | Mobile Equipment |
| METRA | Multi-Element Transmit and Receive Antennas |
| MHGOPA | Modified Hybrid Gradient Optimal Power Allocation |
| MIMO | Multi Input Multi Output |
| MISO | Multi Input Single Output |
| MMSE | Minimum Mean Square Error |
| MoM | Method of Moments |
| MRC | Maximum Ratio Combining |
| NLOS | No Line of Sight |
| NMT | Nordic Mobile Telephone |
| OFDM | Orthogonal Frequency Division Multiplexing |
| OFDMA | Orthogonal Frequency Division Multiple Access |
| OPA | Optimal Power Allocation |
| PA | Power Amplifier |
| PC | Power Control |
| PCC | Primary Carrier Component |
| PDCP | Packet Data Convergence Protocol |
| PHY | Physical Layer |
| PL | Path Loss |
| PRB | Physical Resource Block |
| PSK | Phase Shift Keying |
| QAM | Quadrature Amplitude Modulation |
| RB | Resource Block |
| RF | Radio Frequency |
| RLC | Radio Link Control |
| Rma | Rural Macro-cell |
| RRC | Radio Resource Control |
| Rx | Receiver |
| SCC | Secondary Carrier Component |
| SC-FDMA | Single Carrier Frequency Division Multiple Access |
| SCM | Spatial Channel Model |
| SCME | Spatial Channel Model Extension |
| SHF | Super High Frequency |
| SIC | Successive Interference Cancellation |
| SIMO | Single Input Multiple Output |
| SINR | Signal to Interference-plus-Noise Ratio |

| | |
|---|---|
| SISO | Single Input Single Output |
| SM | Spatial Multiplexing |
| SMa | Suburban Macro-cell |
| SMS | Short Message Service |
| SNR | Signal to Noise Ratio |
| SS | Small Scale |
| sub-CH | Sub-Channel |
| TACS | Total Access Communication System |
| Tx | Transmitter |
| UE | User Equipment |
| UHF | Ultra High Frequency |
| UL | Uplink |
| UMa | Urban Macro-cell |
| UMi | Urban Micro-cell |
| UMTS | Universal Mobile Telecommunications System |
| UTRAN | Universal Terrestrial Radio Access Network |
| V-BLAST | Vertical-Bell Laboratories Layered Space-Time |
| VoIP | Voice over IP |
| W-CDMA | Wideband Code Division Multiple Access |
| Wi-MAX | Worldwide Interoperability for Microwave Access |
| WIM2 | Wireless World Initiative New Radio Phase II Model |
| WINNER | Wireless World Initiative New Radio |
| ZF | Zero Forcing |
| ZIF | Zero Intermediate Frequency |

# 1. INTRODUCTION

The strong demand for wireless broadband services from the growing number of mobile users has been pushing the standards of mobile communication systems to increase the supported peak data rates. In order to meet these demands, the International Telecommunication Union (ITU) has started the standardization of the next generation of mobile communication systems, called IMT-Advanced, or 4G [25]. According to the target performance and technical requirements [26], the new mobile networks should support high data rates up to 1 Gb/s for pedestrian environment and up to 100 Mb/s for high speed environment.

LTE was originally standardized by the 3rd Generation Partnership Project (3GPP) in Release 8 as an evolution of GSM/UMTS standards by offering higher data rates of up to 299.6 Mbit/s (DL) and 75.4 Mbit/s (UL) for 4x4 MIMO, a new flat IP-based network architecture, lower latency (less than 5ms), scalable spectrum bandwidths (1.4 MHz, 3 MHz, 5 MHz, 10 MHz, 15 MHz, and 20 MHz) and use of OFDMA in the DL and SC-FDMA in the uplink for power conserving [8]. Further enhancements for LTE were added in release 9 such as Multimedia Broadcast Multicast Services, LTE-MIMO, dual-layer beam-forming, and femto-cell specifications [2].

For IMT-Advanced, 3GPP has submitted its candidate, LTE-Advanced, in 2009 and was approved and finalized by 3GPP in March 2011. LTE-Advanced promises to meet or even exceed the performance goals set by the ITU for 4G according to the standards of 3GPP in Release 10, while still offering backward compatibility with LTE. The key new technique introduced in LTE-Advanced is the Carrier Aggregation (CA) technique, in which two or more component carriers (CCs) are aggregated, which helps to increase the peak data rate up to 3 Gb/s for DL and 1.4 Gb/s in UL [49].

The introduction of CA in LTE-Advanced poses a challenge to the power control problem with a CA-MIMO radio link. If a user data is being transmitted along different

carrier components (CCs) that are in separate frequency bands, they will experience different channel characteristics in the different CCs. In addition, the use of MIMO will further complicate the problem as each path is considered an independent channel. This will result in a power control problem with multiple power constraints imposed on the mobile equipment: per-CC, per-antenna and per-total transmit power available.

In this thesis, the bit error rate performance of the Modified Hyper Gradient Optimal Power Allocation (MHGOPA) algorithm is analyzed. Four different realistic channel scenarios for a carrier aggregated MIMO radio link is used over a long range of frequencies (2-6 GHz) that cover the most of the frequency bands in 3GPP's feasibility studies of LTE-Advanced [4]. The results of MHGOPA algorithm are compared to the baseline average power allocation algorithm to investigate the achievable improvement in the system performance.

The motivation behind the thesis is the importance of power control optimization in the new CA technique proposed for LTE-Advanced and the lack of algorithms that can handle the different power constraints that CA imposes on the power allocation. The simulations of the algorithm in realistic channel model scenarios should add to the viability of the MHGOPA algorithm and enable us to get more accurate results of its performance.

The flow of the thesis is divided into two parts. The first part, Chapters 2 to 5, covers the theoretical background about Wireless systems, MIMO, CA, power allocation and wireless propagation principles. The second part, Chapter 6, presents the simulation overview and its results. In Chapter 2 we go through a brief history of wireless systems evolution from 1G to LTE, and a brief introduction of the proposed Carrier Aggregation in LTE-Advanced. Chapter 3 gives a brief introduction to the multi-antenna technique of MIMO, then in Chapter 4 we briefly discuss the different power control algorithms and the different scenarios in which these algorithms are viable. Here we also introduce the multiple power constraints problem and the MHGOPA algorithm. In Chapter 5 we give a basic introduction to the principles of wireless propagation. Chapter 6 gives an overview of the simulator used and the WIM2: IMT.ADV channel model. The test scenarios and their parameters are also presented in Chapter 6, followed by the results of

the simulations. Lastly, in Chapter 7, discussion and conclusions based on the obtained results are given.

# 2. WIRELESS SYSTEM EVOLUTION AND CARRIER AGGREGATION

The wireless communications systems have gone through different stages of evolution, commonly known as generations. The 1st Generation of mobile communications were introduced in the 80's and depended on analog communication standards such as Nordic Mobile Telephone (NMT), Advanced Mobile Phone System (AMPS) and Total Access Communications System (TACS).

The next generation, 2G, cellular telecom networks were commercially launched with the GSM standard in 1991. The 2G networks had many advantages over their predecessors since the phone conversations were digitally encrypted. The digital signals between the handsets and the towers increased the system capacity since the digital voice can be compressed and multiplexed much more effectively than analog voice encodings through the use of various codecs, allowing more calls to be packed into the same amount of radio bandwidth. 2G networks also saw the introduction of data services for mobiles like SMS text messages [42].

The evolution from the 2G to 3G occurred in different phases. The main driving factor was to increase the transmission data rates. The first key step in the evolution was the introduction of General Packet Radio Service (GPRS). Wireless network services combined with GPRS became 2.5G, increasing the data rates from 56 kbit/s up to 114 kbit/s. The second key step in the evolution was the progress of GPRS networks to EDGE networks with the introduction of 8PSK encoding. EDGE can be considered a 3G radio technology and is part of ITU's 3G definition, but is most frequently referred to as 2.75G. EDGE was deployed on GSM networks and was standardized by 3GPP as part of the GSM family as an upgrade that provides a potential of three-fold increase in the capacity of GSM/GPRS networks. The specifications achieve higher data-rates by switching to more sophisticated methods of coding (8PSK), within existing GSM timeslots [42].

From EDGE networks the introduction of Universal Mobile Telecommunications System (UMTS) networks and technology marked the beginning of 3G networks. UMTS is based on the International Telecommunication Union (ITU) family of standards under the IMT-2000 and was standardized by 3GPP in release 99 [1]. The UMTS makes use of a new radio interface, the Wideband Code Division Multiple Access (W-CDMA) and required new frequency allocations. The new 3G networks enabled network operators to offer users a wider range of more advanced services while achieving greater network capacity through improved spectral efficiency. Services include wide-area wireless voice telephony, video calls, and broadband wireless data, all in a mobile environment. The first commercial 3G networks were launched by Hutchison Telecommunications in April 2003 [42].

Further upgrades to the UMTS were implemented such as HSPA data transmission capabilities, able to deliver speeds up to 14.4 Mbit/s on the downlink (3GPP release 5) and 5.8 Mbit/s on the uplink (3GPP release 6) through the addition of 16-QAM and 64-QAM modulation, MIMO, link adaptation and fast scheduling. HSPA was further evolved in 3GPP release 7 reaching DL speeds of up to 28.8 Mbps and 11.5 Mbps on UL [22] and became known as HSPA+. Additional improvements to HSPA+ continued in parallel with the introduction of LTE in 3GPP release 8 by adding Duel-Carrier HSDPA and again in 3GPP release 9 by the addition of Duel-Carrier HSDPA with MIMO. The evolution of HSPA+ advanced more with the introduction of Multi-Carrier HSDPA in 3GPP release 10, which can achieve theoretical peak data rates of 168 Mbps (DL) and 23 Mbps (UL), with plans to enhance them more in 3GPP release 11 [37].

## 2.1. Long Term Evolution (LTE)

3GPP LTE (Long Term Evolution) was the name given to the project within the Third Generation Partnership Project to improve the UMTS mobile phone standard to cope with future technology evolutions. The major driving factors for LTE were the increased demand for higher data rates, improving spectral efficiency, lowering costs, improving services, making use of new spectrum and reframed spectrum opportunities, and better integration with other open standards. Although an evolution of UMTS, the LTE air interface is a completely new system based on OFDMA in the downlink and SC-FDMA (DFTS-FDMA) in the uplink that efficiently supports multi-antenna tech-

nologies (MIMO). LTE was designed to support all kind of IP data traffic, including voice over IP (VoIP) in order to enhance the integration with other multimedia services. The architecture that resulted from this work is an all-IP technology called EPS (Evolved Packet System) and comprises E-UTRAN (Evolved UTRAN) on the access side and EPC (Evolved Packet Core) on the core side [6;7;8].

The LTE main objectives and targets achieved can be summarized as follow:

- Increasing peak data rates: Peak data rates target of 100 Mbps (DL) and 50 Mbps (UL) for 20 MHz spectrum allocation, assuming SISO configuration. And up to 299.6 Mbit/s (DL) and 75.4 Mbit/s (UL) for 4x4 MIMO.
- Increased cell edge bit rates: Cell-edge spectrum efficiency of 0.04-0.06 bps/Hz/cell/user (DL) and 0.02-0.03 bps/Hz/cell/user (UL)
- Improve spectrum efficiency: Peak spectrum efficiency of more than 5 bps/Hz (DL) and 2.5 bps/Hz (UL).
- Improve scalability of BW: Scalable bandwidths of 1.3, 3, 5, 10, 15, 20 MHz
- Reduced latency: Less than 5 ms latency
- Reduced power consumption: Power control, link adaptation and use of SC-FDMA in the UL. SC-FDMA is technically similar to OFDMA but better suited for uplink from handheld devices.
- Backward compatibility with earlier releases: The LTE side is easy to integrate with the older network standards, with its network side composed of eNode Bs only. LTE users can also perform calls and access some data services using GSM/GPRS, W-CDMA UMTS or CDMA2000.
- Optimized for low speed mobility, but supporting high speed as well: The LTE is optimized for low speeds (0-15 km/h), but still performs functional for speeds up to 350 km/h or 500 km/h depending on the frequency band used.

The LTE system architecture placed most of the radio functionality fully in the base station. The new functionalities in the Base Transceiver Station (BTS) compared with HSDPA/ HSUPA are now Radio Link Control (RLC) Layer, Radio Resource Control (RRC) and Packet Data Convergence Protocol (PDCP) functionalities. PDCP was first placed in the core network side but was later (early 2007) moved to E-UTRAN (eNode

B). The evolution from UMTS to E-UTRAN is shown in Figure 2.1 while figure 2.2 shows the eNode B and the radio functionality within.

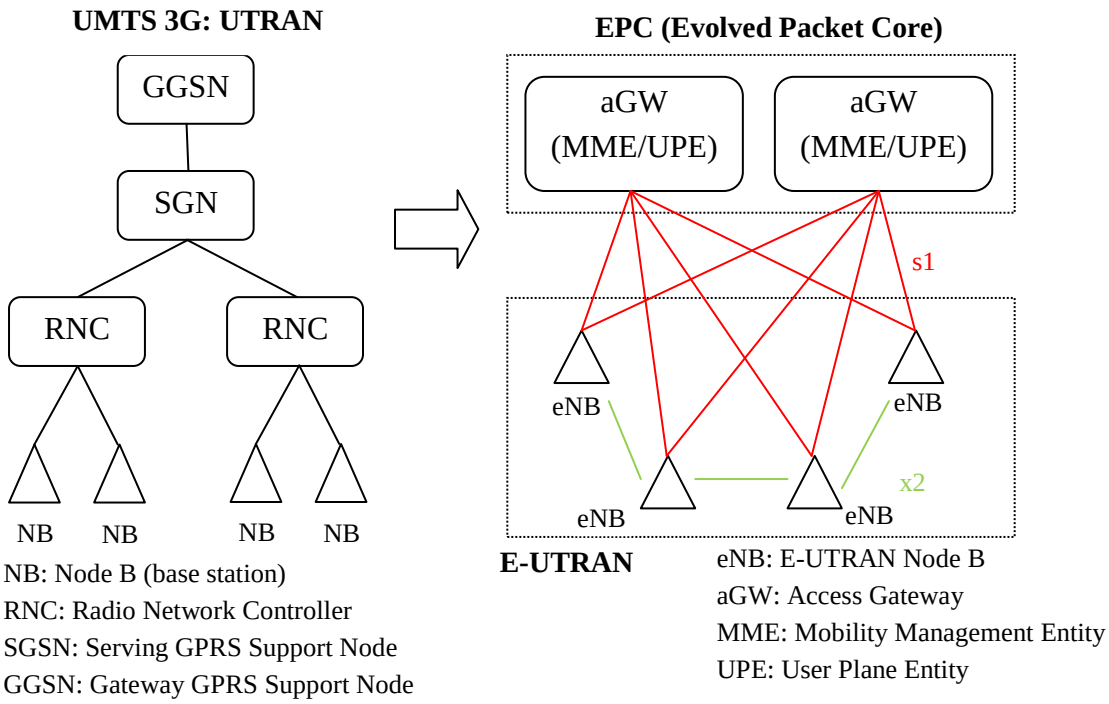


***Figure 2.1*** *Evolution of UMTS into EUTRAN*

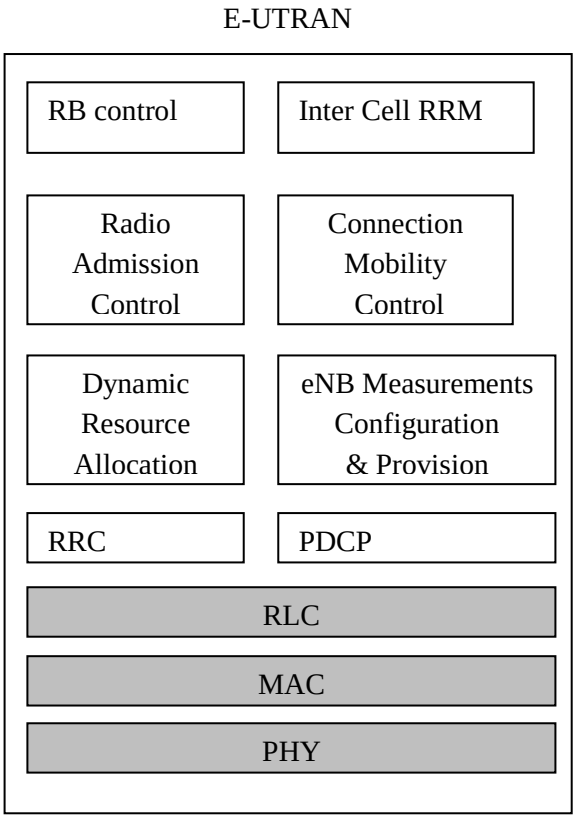


***Figure 2.2*** *Radio functionality in LTE's eNode B*

## 2.2. LTE Advanced

One of the key aspects of next mobile communication systems (4G) is the increase of the data rates to cope with the increased demand for mobile services. Carrier aggregation (CA), in which two or more component carriers (CCs) are aggregated, was proposed by the 3GPP group for their next generation, LTE-Advanced, in order to meet the requirements of the IMT-Advanced systems as shown in Table 2.1 [52].

***Table 2.1*** *Comparison between LTE, LTE-Advanced and IMT-Advanced*

| | **IMT-Advanced** | | **LTE** | | **LTE-Advanced** | |
|---|---|---|---|---|---|---|
| | UL | DL | UL | DL | UL | DL |
| **Peak spectrum efficiency (bps/Hz)** | 6.75 | 15 | >2.5 | >5 | 15 | 30 |
| **Average spectrum efficiency (bps/Hz/cell)** | 1.4 | 2.2 | 0.66-1.0 | 1.6-2.1 | 1.2-2 | 2.4-3.7 |
| **Cell-edge spectrum efficiency (bps/Hz/cell/user)** | 0.03 | 0.06 | 0.02-0.03 | 0.04-0.06 | 0.04-0.07 | 0.07-0.12 |
| **Operating bandwidth (MHz)** | ≤40 | | ≤20 | | ≤100 | |

The use of CA as a technique for increasing the bandwidth for LTE systems comes with many advantages, such as:

- Backward compatibility: The LTE-Advanced will be using the LTE CC as its building block and aggregate two or more to serve as a single unit of LTE-Advanced block.
- Better spectrum utilization by the carrier operators: Since the spectrum resources below 4 GHz are limited, carrier operators can use their currently owned CCs of their old systems to achieve the required data rates, instead of allocating 100 MHz of continuous bandwidth. The different CCs do not need to be of the same bandwidth, which adds to the flexibility and utilization of the scattered small bandwidths.
- Cell Planning: Different cell sizes can be implemented within the same area when using a CC from a different band. This is caused by the fact that higher frequencies will experience more pathloss than lower frequencies.

### 2.2.1. Carrier Aggregation Schemes

LTE-Advanced will support up to 5 CCs, with the LTE CCs bandwidths of 1.4, 3, 5, 10, 15 and 20 MHz for a maximum bandwidth of 100 MHz. The scenarios for CA and its CCs are proposed in [4] as follows:

a) Intra band contiguous CA: The CCs are next to each other as shown in figure 2.3, which have the advantage of less UE complexity, cost, and power consumption. It is also possible to use a single FFT module and a single RF component to achieve the contiguous CA. On the network side, a contiguous CA resource allocation and management algorithm will be simpler.

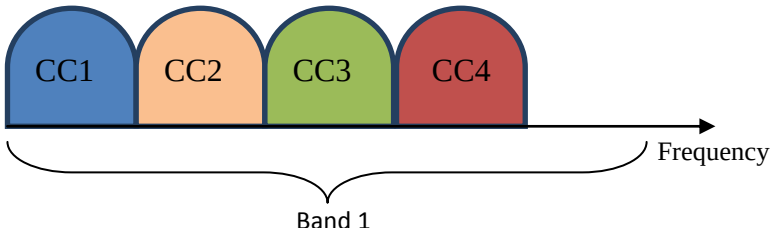


***Figure 2.3*** *Carrier Aggregation: Intra band contiguous*

b) Intra band non-contiguous CA: The CCs are separated among the frequency band as show in figure 2.4. This will require more complexity on the UE and network side, but with the advantage of flexible spectrum allocation for carrier operators, especially since the CCs are not required to be of the same size.

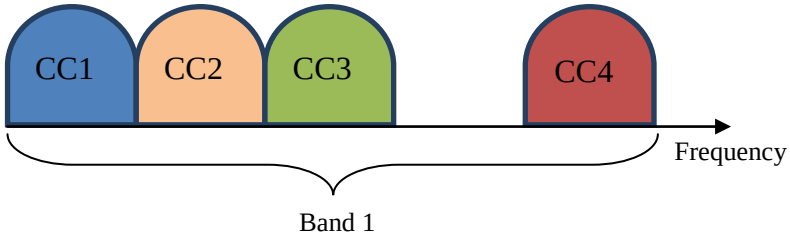


***Figure 2.4*** *Carrier Aggregation: Intra band non-contiguous*

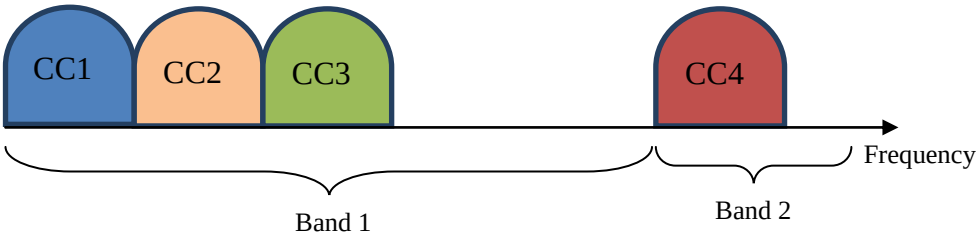


***Figure 2.5*** *Carrier Aggregation: Inter band non-contiguous*

c) Inter band non-contiguous CA: The CCs are located in different frequency bands as shown in figure 2.5. The advantage of this is the ability of utilizing the spectrum of legacy systems such as GSM and 3G. This will require more complexity

for the UE and network to handle the resource allocation and management schemes that will require an adaptive power control, coding and modulation for the different CCs [52].

# 3. MIMO TECHNIQUES FUNDEMENTALS

Multi-antenna techniques' history goes back to the 1970's, where in [13] the capacity of a multi-input multi-output (MIMO) linear channel is derived for a multi-pair telephone cables. Later in the 1990's, spatial multiplexing (SM) with the use of MIMO was proposed in [41] and the first MIMO prototype was demonstrated by Bell Labs in 1998 [20]. The use of MIMO was then adopted commercially in 2001. The system used MIMO with Orthogonal Frequency Division Multiple Access (OFDMA) and supported both diversity coding and spatial multiplexing. Later in 2005, IEEE 802.11n [50] for Wi-Fi was developed, which implemented MIMO within its standards. The MIMO technique was then adopted by many standards such as IEEE802.11e WiMAX broadband [9], HSPA, HSPA+, LTE, and all upcoming 4G systems.

The first benefit of the MIMO was to improve the performance through the diversity gain. The bit error rate (BER) depends on the channel condition and its signal to noise ratio (SNR). By using the diversity principle, as shown in figure 3.1 illustrating a basic MIMO, the Rx receives multiple versions of the same data, each going through a different path with different channel conditions. This results in the reduction of the BER and improves the performance of the radio link. Space diversity added a new dimension to the classical way of transmitting data through time-frequency domain. Spatial multiplexing takes the MIMO a step further by providing additional data rate through utilizing the different paths to carry more data without the knowledge of Channel State Information (CSI), Open-loop approach, or with the knowledge of CSI at the receiver, Closed-loop approach. This increase of channel capacity without increasing the bandwidth makes MIMO technology an important emerging technique [40].

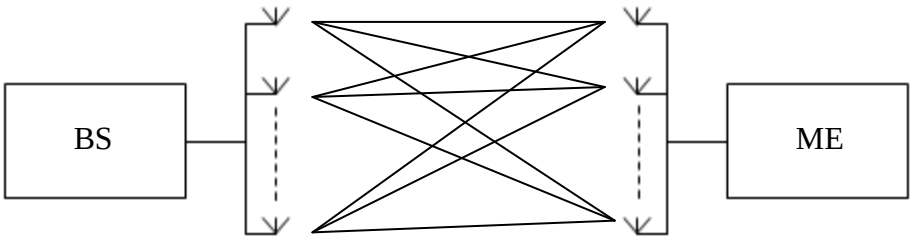


***Figure 3.1*** *Basic MIMO, where each path is considered a different channel*

## 3.1. MIMO Formats

MIMO comes in different formats, depending mainly on the number of antennas on the Tx and Rx sides, as well as the complexity levels. In the MIMO system, the transmitter is considered the input as it transmits the data into the radio link, while the output is the receiver since it receives the data from the output of the radio link. When a transmitter is sending signal vector $\boldsymbol{x}$ through a narrowband flat fading MIMO channel, the received signal $\boldsymbol{Y}$ is modeled as follow:

$$\boldsymbol{Y} = \boldsymbol{H}\boldsymbol{x} + \boldsymbol{n}, \tag{3.1}$$

in which $\boldsymbol{n}$ is the noise vector and the channel matrix $\boldsymbol{H}$ is

$$\boldsymbol{H} = \begin{bmatrix} h_{1,1} & h_{1,2} & \dots & h_{1,N} \\ h_{2,1} & h_{2,2} & \dots & h_{2,N} \\ \vdots & \vdots & \ddots & \vdots \\ h_{M,1} & h_{M,2} & \dots & h_{M,N} \end{bmatrix}, \tag{3.2}$$

where $h_{i,j}$ is the complex channel gain between the receiver antenna $i$ and the transmitter antenna $j$. When speaking of the MIMO channel matrix, most studies include the effects of the RF electronics in the Tx and Rx.

The basic concepts for the different forms of MIMO configurations are shown in figure 3.2. The use of these different formats depends on the application. For example, in some wireless equipment where the battery life is of concern, such as ME's, the use of more than one antenna can be disadvantageous as the more antennas used, the more power needed for transmission and processing. Another factor in the use of the MIMO is the size of ME and whether it can fit the different antennas with the required spacing for the MIMO to be applicable.

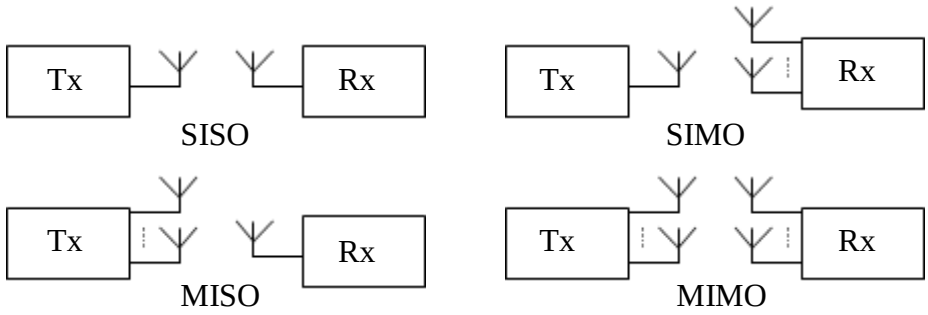


***Figure 3.2*** *Different antenna configurations*

### 3.1.1. Single Input Single Output (SISO)

The single input single output (SISO) is the simplest antenna configuration, which is also the most basic wireless link. It is basically a normal radio link with one operating antenna on both the transmitter and receiver side. The SISO therefore does not need any extra processing unless other forms of diversity are used with it, such as frequency and/or time diversity. Given that the SISO system consists of one radio link, and therefore one radio channel, the system will be more vulnerable to interference and fading than a MIMO with some form of diversity. Finally, the channel capacity will be limited by Shannon's law depending on the bandwidth used and channel SNR. The channel matrix $\boldsymbol{H}$ of a SISO link is simply represented by a single channel gain element:

$$\boldsymbol{H} = [h_{1,1}], \tag{3.3}$$

### 3.1.2. Single Input Multiple Output (SIMO)

The single input multiple output, or SIMO configuration is when the transmitter has a single antenna while the receiver has multiple antennas. Since most of the power consumption and processing is done in the receiver end and the transmitter remains simple, we see this type of configuration most common in mobile networks Uplinks (UL) where the ME is usually transmitting with a single antenna to a BS with multiple receiving antennas. This technique, receiver diversity, enables the receiver to minimize the effects of fading through diversity. The two main diversity methods for SIMO are Switched diversity and Maximum Ratio Combining (MRC). Switched diversity is the simplest to implement. The receiver basically searches for the antenna with the best SNR and switches to it. The MRC on the other hand is an optimum method but harder to implement. The MRC combines all the received signals linearly to maximize the SNR of the received signal. Therefore all antennas contribute to the overall signal with knowledge of CSI in the receiver. The channel matrix $\boldsymbol{H}$ of a SIMO link is represented by a channel gain column-vector:

$$\boldsymbol{H} = \begin{bmatrix} h_{1,1} \\ h_{2,1} \\ \vdots \\ h_{M,1} \end{bmatrix}, \tag{3.4}$$

### 3.1.3. Multiple Input Single Output (MISO)

The multiple input single output (MISO) configuration is when the transmitter has multiple antennas while the receiver has a single antenna. Through the use of space-time coding or frequency coding techniques, specific codes can be combined with the transmit diversity at the cost of data-rates without the need of CSI. A common and simple method is the Alamouti's code, which is designed for two antenna branches that provides a diversity order equal to MRC in the case of SIMO [10] with coding rate 1 (no loss in data rates). In this form the extra processing is done in the transmitter end, which is beneficial to mobile networks in the Downlink (DL) since the BS does have continuous power supply and higher processing power than the receiver. The channel matrix $\boldsymbol{H}$ of a MISO link is represented by a channel gain row-vector:

$$\boldsymbol{H} = \left[h_{1,1}\ h_{1,2}\ \ldots\ h_{1,N}\right], \tag{3.5}$$

### 3.1.4. Multiple Input Multiple Output (MIMO)

The last form is the multiple input multiple output (MIMO) in which both sides of a radio link have more than one antenna. This form can provide robustness to the radio link (diversity) as well as an increase in the transmission rate (Spatial Multiplexing) if the channel is rich in scatters and the antennas are sufficiently spaced. The Spatial Multiplexing can be realized by splitting the data to different groups to be sent through each antenna. The first approach to Spatial Multiplexing is the Open-loop approach that doesn't require CSI on the transmitter side but require proper equalizer/detector on the receiver side in order separate the streams and detect the symbols correctly. The other approach, Closed-loop approach, depends on CSI in the transmitter side and the utilization of pre-coding to give improvement over the Open-loop approach. In order for the receiver to recover all the data transmitted, the number of the receiver antennas should be equal to the transmitter (or higher to achieve extra receiver diversity). If the need is for more link robustness instead of spectral efficiency, the transmit and/or receive-diversity discussed earlier can be combined with MIMO.

The use of the full MIMO gives the best results in case of improved performance and throughput, but the complexity is increased greatly due to the extra processing that needs to be done on both transmitter and receiver. The channel matrix $\boldsymbol{H}$ of a MIMO link is represented as shown previously in equation (3.2).

### 3.1.5. MIMO and Multicarrier Techniques

Earlier in 3.1 when discussing the MIMO channel, we presented the channel as a matrix of complex gain values. This means that for each path, the frequency response over the signal transmission bandwidth is assumed to be flat. The MIMO channel in literature is usually modeled to be narrowband flat fading channel, otherwise the modeling will get very complex if we take into consideration time-domain dispersion. In multicarrier techniques, such as OFDM, the transmission bandwidth is divided into narrow subcarriers (15 kHz subcarrier spacing in LTE), therefore each subcarrier channel can be considered a narrowband flat fading channel with a constant frequency response. This makes the MIMO a good match with multicarrier techniques such as the OFDM.

# 4. CA MIMO RADIO LINK MODEL AND CONSTRAINED POWER ALLOCATION OPTIMIZATION

The combined use of multiple antennas and CA in LTE-Advanced, as shown in figure 4.1, gives the system the opportunity to deal with the limited frequency resources and presents us with a CA-MIMO radio link with a major challenge for power control (PC) optimization. The CA-MIMO radio link will experience different channel characteristics for the different CCs, and in the system deployment, the CA-MIMO link will have multiple power constraints: per-CC, per-antenna and total transmission power constraint. The optimization of the power control for the CA-MIMO link with the mentioned constraints is essential for the link performance in LTE-Advanced network scenarios.

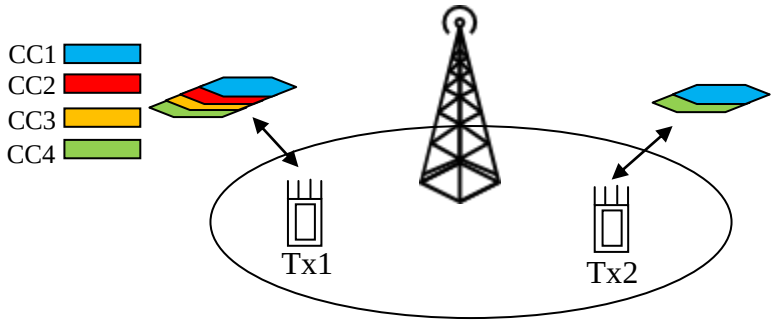


***Figure 4.1*** *A general CA-MIMO network*

## 4.1. CA Scenarios

The LTE-Advanced is based on LTE standards with the main addition of carrier aggregation. As mentioned previously, the CA schemes can results in *contiguous* CCs within the same frequency band, or *non-contiguous CCs* that can be within the same frequency band or spread over a long range of frequencies (800 MHz-6 GHz). The users multiple sub-channels (sub-CHs) that make up the physical resource block (PRB) set in LTE-Advanced will therefore experience different radio channel characteristics depending on the frequency. At the same time, the spatial sub-CHs that results from the use of MIMO will further deepen the channel characteristics differences [51].

Given the differences in the channel characteristics owing to the varying channel conditions over frequency and spatial domains, an optimal PC policy for CA-MIMO radio links that divide the transmission power between CCs and antennas according to the channel characteristics is therefore needed.

For a transmitter to support one or more of the carrier aggregation schemes, four physical implementations options of a transmitter architecture are possible and are presented in the LTE-Advanced feasibility study in [4]:

- *Option A:* This simple transmitter architecture with a single PA can only support one mode of CA: Intra Band Contiguous. Intra Band Non-Contiguous and Inter Band Non-Contiguous are not supported. The reason being that all the processing is done in a single chain where the CCs are multiplexed before going through a wideband IFFT, a wideband DAC and a zero-IF (ZIF) mixer as shown in figure 4.2.

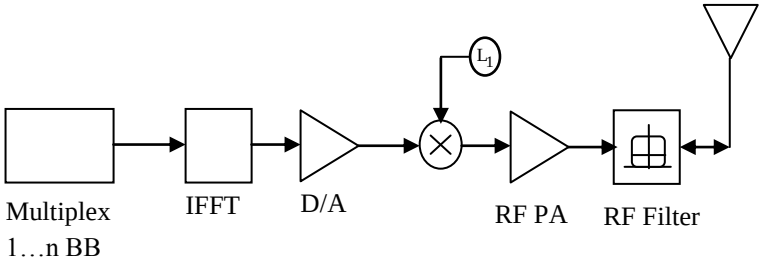


***Figure 4.2*** *Transmitter architecture for option A*

- *Option B:* The transmitter in this case have the different CCs processed independently at the baseband through IFFT, DAC and a mixer operating at an IF of around the bandwidth of the second CC ( 2 CCs example). The wideband signal is then up-converted to RF as shown in figure 4.3. In this architecture both Contiguous and Non-Contiguous Intra-band CA can be supported. As the Tx has a single PA, it cannot support Inter Band Non-Contiguous CA.

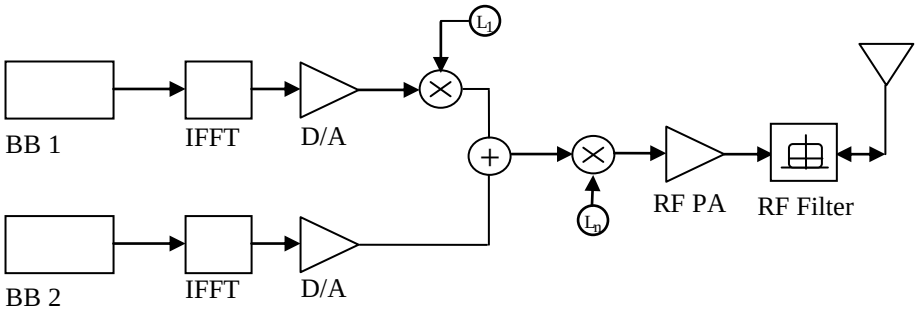


***Figure 4.3*** *Transmitter architecture for option B*

- Option C: The transmitter in this architecture similar to the architecture of option B, but does a ZIF up-conversion of each CC before combining and feeding the signal into the PA as shown in figure 4.4. The architecture of this transmitter is capable of operating both Intra Band CA schemes (Contiguous and Non-Contiguous), but cannot support Inter Band CA.

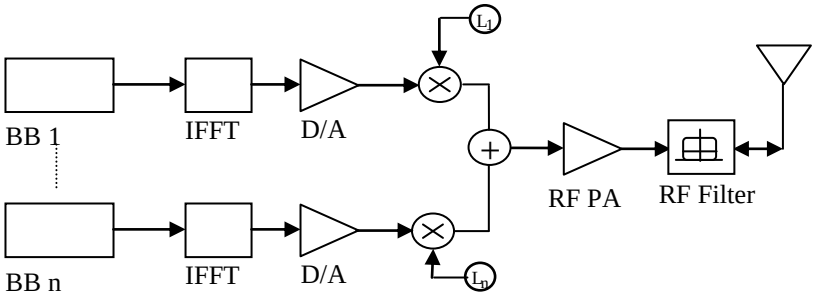


***Figure 4.4*** *Transmitter architecture for option C*

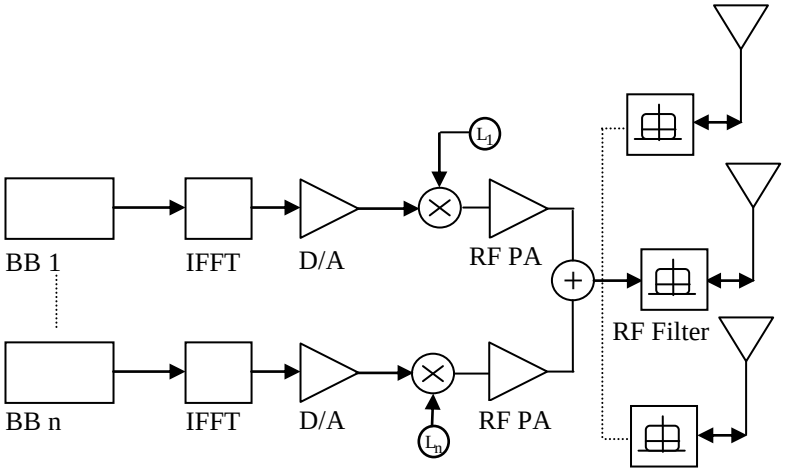


***Figure 4.5*** *Transmitter architecture for option D*

- Option D: This architecture is capable of taking full advantage of the three CA schemes, as it supports both Intra Band and Inter Band CA. The transmitter in this case uses multiple RF chains with multiple PAs to process the CCs. The signals are then combined with a high-power combiner and fed to the antenna(s) as shown in figure 4.5.

The above mentioned options give rise to four different CA scenarios when we look at the PC problem and the power constraints associated with it. The four scenarios are classified in table 4.1. The simplest configuration is for a CC-SISO/SIMO system where only a single CC and a single antenna are present in the transmitter. An optimum power

allocation and control algorithms were developed in [38] that minimize the sum of the transmitted power of all the users in multiple access channel while ensuring the target data rates are maintained. In such a scenario, the PC algorithm will have to deal only with the single constraint: Tx power budget.

***Table 4.1*** *Configuration for basic CA scenarios*

| Scenario No. | System | CC No. | PA. | Power Limit | | |
|---|---|---|---|---|---|---|
| | | | | Per-CC | Per-PA | Per-Tx |
| 1 | CC-SISO/SIMO | 1 | 1 | No | No | Yes |
| 2 | CC-MIMO | 1 | >1 | No | Yes | Yes |
| 3 | CA-SISO/SIMO | >1 | 1 | Yes | No | Yes |
| 4 | CA-MIMO | >1 | >1 | Yes | Yes | Yes |

For the second scenario, CC-MIMO system, multiple algorithms in literature are available to deal with the per-antenna power constraint. Opportunistic Power Control [43] and V-BLAST power control with per-antenna power constraints [19] have maximized the overall throughput of the multi-user MIMO-OFDM system with a fixed total transmit power, while the optimal power allocation (OPA) schemes proposed in [34] and [16] have minimized the bit error rate (BER) averaged over all the CC-MIMO antennas subject to a predefined total power budget. Further improvements to the CC-MIMO system were achieved in [35] and [47].

For CA systems, a system level uplink power allocation algorithm was developed in [48]. This algorithm considers a CA system with multiple CCs and three types of users in the system: LTE Rel.8 user, power-limited LTE-Advanced user, and non-power-limited user. The algorithm functions by simply allocating a single CC to LTE Rel.8 or power-limited LTE-Advanced users, while possibly assigning multiple CCs to non-power-limited users, therefore making it applicable to CA-SISO/SIMO configuration only. CA-MIMO is not applicable since per-antenna constraints aren't considered.

The last configuration for a basic CA system is CA-MIMO. In this scenario, the PC will have to deal with per-CC, per-antenna and per-Tx power constraints, which make the power allocation more difficult. In addition to the different channel characteristics of each CC, the CA-MIMO system will require more specific CC constraints due to the use of different power levels for Primary CC (PCC) and Secondary CC (SCC).

## 4.2. Multiple Power Constraints Problem

In this section, we will consider a single CA-MIMO radio link between (Tx-BS) aggregating *K* CCs sharing all the available *N* transmit antennas, with *M* antennas at the receiver. It is assumed that the Tx is using a single OFDM sub-CH per-CC. In the following analysis, bold characters denote a column vector as default. **1**, **0** indicate column vector of either ones or zeros. $\|.\|$ denotes the Euclidean norm of the enclosed vector and $|.|$ indicate the amplitude of the enclosed complex value. $\boldsymbol{I}_N$ denotes the $N \times N$ identity matrix and row($\boldsymbol{A}$), n($S$) are the number of rows in the matrix $\boldsymbol{A}$ and the entry number in the set $S$, respectively. Finally, $E\{.\}$ denotes the expectation and (.) for the transposition [17].

For a CA-MIMO single Tx case, the received signal vector for the *j*th CC is:

$$\boldsymbol{Y}_j = \boldsymbol{H}^j_{M\times N}\sqrt{\boldsymbol{P}_j}\boldsymbol{X}_j + \boldsymbol{n}_j, \quad j = (1,2,\dots,K). \tag{4.1}$$

1) The variable $\boldsymbol{Y}_j = \left[y_{(1,j)},\dots,y_{(M,j)}\right]^T$ represents the received symbol vector from all the *M* receiver antennas for the *j*th CC. The total received signal will be $\boldsymbol{Y}_{M\times K} = \left[\boldsymbol{Y}_1,\dots,\boldsymbol{Y}_j,\dots,\boldsymbol{Y}_K\right]$.
2) $\boldsymbol{H}^j_{M\times N} = \left[\boldsymbol{h}^j_1,\dots,\boldsymbol{h}^j_i,\dots,\boldsymbol{h}^j_N\right]^T$ is the channel matrix, whose element $\boldsymbol{h}^j_i$ is a column vector that represent the channel gains from *i*th transmit antenna to the *M* receiver antennas. When taking the CCs into consideration, we get the channel matrices $\boldsymbol{H}_{M\times N\times K} = \left[\boldsymbol{H}^1_{M\times N},\dots.,\boldsymbol{H}^j_{M\times N},\dots.,\boldsymbol{H}^K_{M\times N}\right]$ whose characteristics depend greatly on the used center-frequency of each CC.
3) $\boldsymbol{P}_j = diag\left(p_{(1,j)},\dots,p_{(i,j)},\dots,p_{(N,j)}\right)$ denotes the transmission power matrix whose element $p_{(i,j)}$ stands for the transmission power of the *i*th symbol in the *j*th CC. The full transmission power matrix for all the symbols in every CC is $\boldsymbol{P}_{N\times N\times K} = \left[\boldsymbol{P}_1,\dots,\boldsymbol{P}_j,\dots\boldsymbol{P}_K\right]$.
4) $\boldsymbol{X}_j = \left[x_{(1,j)},\dots,x_{(i,j)},\dots,x_{(N,j)}\right]^T$ denotes the transmit symbol vector for the *j*th CC employing all the *N* transmit antennas whose element $x_{(i,j)}$ is drawn independently from a common constellation with a unit average power: $E\left\{\left|x_{(i,j)}\right|^2\right\} = 1$. The full transmitted signal over all the *K* CCs is $\boldsymbol{X}_{N\times K} = \left[\boldsymbol{X}_1,\dots,\boldsymbol{X}_j,\dots,\boldsymbol{X}_K\right]$.

5) $\boldsymbol{n}_j = \left[n_{(1,j)}, \dots, n_{(M,j)}\right]^T$ denotes the *M*-dimensional noise vector whose elements are independent and identically distributed (i.i.d) complex Gaussian random variables with zero mean and a variance of $\sigma^2$: $E\left\{\boldsymbol{n}_j\left(\boldsymbol{n}_j\right)^H\right\} = \sigma^2\boldsymbol{I}_M$.

The study assumes that the decoding in the Rx is CC-specific, with the inter-CC interference neglected. The ideal successive interference cancellation (SIC) and fixed detection order in [19] are assumed. The approximation for the post detection signal to interference-plus-noise ratio (SINR) for symbol *i* in the *j*th CC is:

$$SINR_{(i,j)} = p_{(i,j)}g_{(i,j)}, \tag{4.2}$$

where

$$g_{(i,j)} = \begin{cases} \dfrac{\left|\left[\boldsymbol{F}_j\right]_i \boldsymbol{h}_i^j\right|^2}{\sigma^2\left\|\left[\boldsymbol{F}_j\right]_i\right\|^2 + \sum_{l=1}^{i-1}\left|\left[\boldsymbol{F}_j\right]_i \boldsymbol{h}_l^j\right|^2}, & MMSE \\ \dfrac{1}{\sigma^2\left\|\left[\boldsymbol{F}_j\right]_i\right\|^2}, & ZF \end{cases} \tag{4.3}$$

The variable $\boldsymbol{F}_j$ is the linear MMSE or ZF filter with $\boldsymbol{P}_j = \boldsymbol{I}_N$, and $g_{(i,j)}$ is the post detection SINR for the case of $p_{(i,j)} = 1$. Since the transmitted symbols are independent of one another, the overall uncoded BER can be calculated as average of the BER of every symbol:

$$\bar{P}_E = \frac{1}{NK} f(p_{(i,j)}), \tag{4.4}$$

where $f\left(p_{(i,j)}\right) = \sum_{i=1}^{N}\sum_{j=1}^{K} \alpha e^{(-\beta SINR_{(i,j)})}$. The variables $\alpha$ and $\beta$ are the constellation specific constants of the uncoded R-ary quadrature amplitude modulation (QAM) from [35] with the values $\alpha = 0.2$ and $\beta = 3/2(2^R - 1)$ for all the employed symbols.

Since we want to minimize the average uncoded BER shown in (4.4) and *N* and *K* are constants. The only variable that can be modified is $f\left(p_{(i,j)}\right)$. Therefore the power allocation that minimizes the average uncoded BER with CC, PA, and Tx constraints is

$$\begin{aligned} &\left\{p_{(i,j)}\right\}_{i=\{1,\dots,N\}}^{j=\{1,\dots,K\}} = \arg\min f\left(p_{(i,j)}\right) \\ &\text{subject to } \sum_{j=1}^{K} p_{(i,j)} \le P_i^A, \sum_{i=1}^{N} p_{(i,j)} \le P_j^C, \\ &\qquad P_i^A \le \sum_{j=1}^{K} P_j^C = P^T \le \sum_{i=1}^{N} P_j^A, \\ &\qquad p_{(i,j)} \ge 0, \quad j = (1,2,\dots,K), \quad \forall 1 \le i \le N, \end{aligned} \tag{4.5}$$

where $P_i^A$ is the *i*th antenna's power constraint, $P_j^C$ denotes the power constraint of the *j*th CC and finally, $P^T$ is the total power limit of the Tx.

The linear constraints in Eq. (4.5) can be mapped into the following inequalities:

$$\boldsymbol{Ap} \geq \boldsymbol{b}, \tag{4.6}$$

where $\boldsymbol{A} = [\boldsymbol{a}_j, j \in S]^T, S = \{1, \dots, N + K + NK\}, \boldsymbol{a}_j \in \mathbb{R}^{NK}$.
$\boldsymbol{b} = -[P_1^A, \dots, P_N^A, P_1^C, \dots, P_K^C, \boldsymbol{0}]^T$, $\boldsymbol{0} \in \mathbb{R}^{NK}$. And the non-negative variables $\boldsymbol{p} = [p_{(1,1)}, \dots, p_{(N,K)}]^T$.

## 4.3. MHGOPA Algorithm

An optimal solution to equation (4.5) that can provide an optimal power allocation for a CA-MIMO radio link was proposed in [17]. The proposed modified hybrid gradient optimal power allocation (MHGOPA) algorithm is a combination of the gradient projection method (GPM) and the conjugate gradient method (CGM). Within the MHGOPA, the GPM algorithm performs an iterative algorithm appropriate for solving equation (4.6), a non-linear problems with linear constraints. For the single Tx CA-MIMO scenario, equation (4.6) can be rewritten as

$$\begin{bmatrix} \boldsymbol{A^1} \\ \boldsymbol{A^2} \end{bmatrix} \boldsymbol{p} \geq \begin{bmatrix} \boldsymbol{b}^1 \\ \boldsymbol{b}^2 \end{bmatrix}, \tag{4.7}$$

where

1) $\boldsymbol{A}^1 = -\begin{bmatrix} \boldsymbol{B}_{N\times K}^1 & \dots, & \boldsymbol{B}_{N\times K}^N \\ \boldsymbol{I}_K & \dots, & \boldsymbol{I}_K \end{bmatrix}$ is composed of the rows of working constraints, $\boldsymbol{B}_{N\times K}^i = \left[\underbrace{\boldsymbol{0}, \dots, \boldsymbol{0}}_{i-1}, \boldsymbol{1}, \underbrace{\boldsymbol{0}, \dots, \boldsymbol{0}}_{N-i}\right]^T$ is composed of rows that point to the values of the symbol powers $p_{(i,j)}$ in $\boldsymbol{p}$ for each CC in the *i*th antenna, while the identity matrices $\boldsymbol{I}_K$ is composed of rows that point to the values of the symbol powers $p_{(i,j)}$ of $\boldsymbol{p}$ for each antenna in the *j*th CC. $\boldsymbol{A}^2 = \boldsymbol{I}_{NK}$.
2) $\boldsymbol{b}^1 = [P_1^A, \dots, P_N^A, P_1^C, \dots, P_K^C]$ represent the fixed constraint values for each CC and antenna, and $\boldsymbol{b}^2 = \boldsymbol{0} \in \mathbb{R}^{NK}$

The main idea is to find the feasible direction that, at each iteration which improves the objective value, aims toward the optimal solution by projecting the gradient direction to the null space of the active constraint matrix, by creating the projection matrix $\mathrm{M}_1$.

$$\boldsymbol{d}'^{(n)} = \boldsymbol{M}_1 \boldsymbol{g} \tag{4.8}$$

where,

1) $\boldsymbol{d}'^{(n)}$ is the feasible direction
2) $\boldsymbol{M}_1$ is the projection matrix, i.e., the solution space of $A_1 x = 0$ and can be calculated as:

$$\boldsymbol{M}_1 = \boldsymbol{I}_{NK} - \boldsymbol{A}_1^T (\boldsymbol{A}_1 \boldsymbol{A}_1^T)^{-1} \boldsymbol{A}_1 \tag{4.9}$$

3) $\boldsymbol{g}$ is the gradient direction: $\boldsymbol{g} = -\nabla f(\boldsymbol{p}^{(n)})$
4) $\boldsymbol{A}_1 = [\boldsymbol{a}_j, j \in S_1]^T$, $S_1 \subset S$ and $\boldsymbol{b}_1 = [\boldsymbol{b}]_{S_1}$ is defined as the active constraint matrix of $\boldsymbol{A}$, such that for a given feasible point $\boldsymbol{p}^0$:

$$\boldsymbol{A}_1 \boldsymbol{p}^0 = \boldsymbol{b}_1 \tag{4.10}$$

The GPM algorithm works for the case that the active constraint matrix $\boldsymbol{A}_1$ is always non-degenerate, as in $\text{rank}(\boldsymbol{A}_1) = \text{row}(\boldsymbol{A}_1)$. In the case $\boldsymbol{A}_1$ is degenerate, for the case of $\text{rank}(\boldsymbol{A}_1) < row(\boldsymbol{A}_1)$, it was verified in [17] that the GPM still holds IFF $\exists\, \text{J}^* \subset \{1, 2, \dots, \text{K}\}$, $\text{I}^* \subset \{1, 2, \dots, \text{N}\}$ such that:

$$\sum_{j=1, j \notin J^*}^{K} P_j^C = \sum_{i=1, i \notin I^*}^{N} P_i^A \tag{4.11}$$

where $J^*$ and $I^*$ denotes the shut down sets of CCs and antennas respectively. The two cases of $\boldsymbol{A}_1$ are discussed briefly in the next subsections.

### 4.3.1. Power Allocation Algorithm with non degenerate $\boldsymbol{A}_1$

As mentioned earlier, the GPM algorithm holds for when $rank(\boldsymbol{A}_1) = row(\boldsymbol{A}_1)$, i.e., non-degenerate $\boldsymbol{A}_1$. The uncoded BER for each symbol $f(p_{(i,j)})$ is a monotonically decreasing function and since the power of all the CCs should never be greater than the collective antennas power, the problem can be revised as:

$$\begin{gathered} max\{-f(\boldsymbol{p})\} \\ \text{Subject to } [\boldsymbol{A}]_{[N+1,\dots,N+K]} \boldsymbol{p} = [\boldsymbol{b}]_{[N+1,\dots,N+K]}, \\ [\boldsymbol{A}]_{S/[N+1,\dots,N+K]} \boldsymbol{p} \geq [\boldsymbol{b}]_{S/[N+1,\dots,N+K]} \end{gathered} \tag{4.12}$$

As consistent with equations (4.8) and (4.9), at the *n*th iteration of the algorithm (Table 4.2):

1) If the feasible point $\boldsymbol{p}^{(n)}$is within the feasible region, then $\boldsymbol{A}_1$ is null, $\boldsymbol{M}_1 = \boldsymbol{I}_{NK}$ and therefore the feasible direction $\boldsymbol{d}'^{(n)} = \boldsymbol{g} = -\nabla f\left(\boldsymbol{p}^{(n)}\right)$.
2) Otherwise if the feasible point is located at the boundary of the feasible region, then the feasible direction is $\boldsymbol{d}'^{(n)} = \boldsymbol{M}_1\boldsymbol{g} = (\boldsymbol{I}_{NK} - \boldsymbol{A}_1^T(\boldsymbol{A}_1\boldsymbol{A}_1^T)^{-1}\boldsymbol{A}_1)\left(-\nabla f\left(\boldsymbol{p}^{(n)}\right)\right)$.

***Table 4.2*** *MHGOPA Algorithm [17]*

| | |
|---|---|
| Step 1. | Initial decomposition:<br>$\boldsymbol{A} = \begin{bmatrix}\boldsymbol{A_1}\\ \boldsymbol{A_2}\end{bmatrix}, \boldsymbol{b} = \begin{bmatrix}\boldsymbol{b_1}\\ \boldsymbol{b_2}\end{bmatrix}$<br>$\boldsymbol{A_1 p^{(n)}} = \boldsymbol{b_1}, \boldsymbol{S_1'} = \{\boldsymbol{N+1}, \dots, \boldsymbol{N+K}\} \in \boldsymbol{S_1}$,<br>$\boldsymbol{A_2 p^{(n)}} > \boldsymbol{b_2}$, $\boldsymbol{A_2} = \left[\boldsymbol{a_j}, \boldsymbol{j} \in \boldsymbol{S_2}\right]^{\boldsymbol{T}}$, $\boldsymbol{S_2} = \boldsymbol{S}/\boldsymbol{S_1}$ |
| Step 2. | Projection Matrix:<br>$\boldsymbol{M}_1 = \boldsymbol{I}_{NK} - \boldsymbol{A}_1^T\boldsymbol{U}_1 = \boldsymbol{I}_{NK} - \boldsymbol{A}_1^T(\boldsymbol{A}_1\boldsymbol{A}_1^T)^{-1}\boldsymbol{A}_1$ |
| Step 3. | Initial direction:<br>$\boldsymbol{d}'^{(n)} = \boldsymbol{M}_1\boldsymbol{g} = -\boldsymbol{M}_1\nabla f\left(\boldsymbol{p}^{(n)}\right)$ |
| Step 4. | Deciding Vector:<br>If $\boldsymbol{d}'^{(n)} \neq 0$, go to step 6<br>Else, $\boldsymbol{\omega}_1 = \boldsymbol{U}_1\boldsymbol{g} = \left[\omega_1^i, i \in \boldsymbol{S_1'}\right]^T$ |
| Step 5. | If $\boldsymbol{\omega_1'} = \left[\omega_1^i, i \in S_1 \backslash \boldsymbol{S_1'}\right]^T \leq \boldsymbol{0}$, stop.<br>Else $\omega_1^{i'} = \max\{\omega_1^i \vert \omega_1^i, i \in S_1 \backslash \boldsymbol{S_1'}\}$<br>$\boldsymbol{A^1} = \left[\boldsymbol{a}_j, i \in S_1 \backslash i'\right]^T$<br>Go back to Step 2. |
| Step 6. | Final Direction:<br>$\varsigma^{(n-1)} = \left\|\boldsymbol{d}'^{(n)}\right\|^2 / \left\|\boldsymbol{d}'^{(n-1)}\right\|^2$<br>$\boldsymbol{d}^{(n)} = \begin{cases}\boldsymbol{d}'^{(n)} + \varsigma^{(n-1)}\boldsymbol{d}^{(n-1)}, & n \geq 2\\ \boldsymbol{d}'^{(n)}, & n = 1\end{cases}$ |
| Step 7. | Step size:<br>$\begin{cases}-f\left(\boldsymbol{p}^{(n)} + \lambda^{(n)}\boldsymbol{d}'^{(n)}\right) + f\left(\boldsymbol{p}^{(n)}\right) \geq \rho\lambda^{(n)}\boldsymbol{g}^T\boldsymbol{d}^{(n)},\\ -f\left(\boldsymbol{p}^{(n)} + \lambda'^{(n)}\boldsymbol{d}'^{(n)}\right) + f\left(\boldsymbol{p}^{(n)}\right) < \varsigma\lambda'^{(n)}\boldsymbol{g}^T\boldsymbol{d}^{(n)},\end{cases}$<br>$\lambda^{(n)} = \psi\lambda'^{(n)}$<br>$0 < \rho, \varsigma < 1, \psi > 0$<br>$0 \leq \lambda^{(n)} \leq \lambda_{max}$<br>$\lambda_{max} = \begin{cases}\infty, & \boldsymbol{d'} \geq \boldsymbol{0}\\ min\left\{\frac{\hat{b}_i}{\hat{d}_i} \vert \boldsymbol{d}_i' < 0\right\}, & else\end{cases}$<br>$\boldsymbol{b'} = \left[\hat{b}_i, i \in S_2\right]^T = \boldsymbol{b}_2 - \boldsymbol{A}_2\boldsymbol{p}^{(n)}$<br>$\boldsymbol{d'} = \left[\hat{d}_i, i \in S_2\right]^T = \boldsymbol{A}_2\boldsymbol{d}^{(n)}$ |
| Step 8. | Next loop:<br>$\boldsymbol{p}^{(n+1)} = \boldsymbol{p}^{(n)} + \lambda^{(n)}\boldsymbol{d}^{(n)}$<br>$n \leftarrow n + 1$ |

Since $[\boldsymbol{A}]_{[N+1,\dots,N+K]}\boldsymbol{p} = [\boldsymbol{b}]_{[N+1,\dots,N+K]}$, and $S_1' = \{N+1, \dots, N+K\}$ where $S_1'$ is a subset of $S_1$, then $\boldsymbol{A}_1$ can never be an empty matrix. As the MHGOPA algorithm's iterations keep going, the feasible point $\boldsymbol{p}^{(n)}$ moves toward an optimum until the next two conditions are met:

1) $\boldsymbol{d}'^{(n)} = 0$
2) The deciding vector's elements $\left[\omega_1^i, i \in S_1 \backslash S_1'\right]^T$ are all negative, where $\boldsymbol{\omega}_1 = \left[\omega_1^i, i \in S_1\right]^T = (\boldsymbol{A}_1\boldsymbol{A}_1^T)^{-1}\boldsymbol{A}_1\boldsymbol{g}$.

In the case that only the first condition is satisfied, then the algorithm will remove the i′th row of $\boldsymbol{A}_1$ and the algorithm will go back to step 2, where $\mathrm{i}' \in \mathrm{S}_1 \backslash \mathrm{S}_1'$ and $\omega_1^{\mathrm{i}'} = \max\{\omega_1^{\mathrm{i}} | \omega_1^{\mathrm{i}}, \mathrm{i} \in \mathrm{S}_1 \backslash \mathrm{S}_1'\}$.

The MHGOPA algorithm makes use of the Fletcher-Reeves conjugate gradient method [18] with an inexact line search of Goldstein [32] in order to increase the convergence. The step size is determined by the Goldstein line search, which make sure that the step size neither too large nor too small and the final direction $\boldsymbol{d}^{(n)}$ at each iteration (step 6) makes use of the Fletcher-Reeves method.

### 4.3.2. Power Allocation Algorithm with degenerate $\boldsymbol{A_1}$

In the case that $\boldsymbol{A}_1$ is degenerate, i.e., $rank(\boldsymbol{A}_1) \neq row(\boldsymbol{A}_1)$, we can still apply the MHGOPA algorithm by substituting $\boldsymbol{A}_1$ with one of its basis as proven in [17]. First we pick a random basis of $\boldsymbol{A}_1$ called $\boldsymbol{A}^+$ with row basis $S^+$. Then we try to find the feasible point $\boldsymbol{p}^* \in \mathbb{R}^{NK}$ with one specific basis $\boldsymbol{A}^*$ such that our two conditions for an optimum are met. Basically, the initial direction $\boldsymbol{d}'^{(n)} = \boldsymbol{M}^*\boldsymbol{g} = \boldsymbol{0}$ and the deciding vector $\boldsymbol{\omega}^* \leq 0$ should be satisfied simultaneously. The step by step algorithm for finding the optimum basis is shown in table 4.3.

Simulations for the performance of the MHGOPA algorithm for a CA-MIMO radio link will be evaluated through Matlab simulations in Chapter 6 for various scenario environments after a short introduction of channel modeling in Chapter 5.

***Table 4.3*** *Optimum basis selection algorithm [17]*

| | |
|---|---|
| Step 1. | Initial equation:<br>$\boldsymbol{A_1^T y = v}$<br>subject to: $\boldsymbol{y = \left[y_j, j \in \{1, 2, \dots, n(S_1)\}\right]^T}$<br>$\boldsymbol{v = -(A^+)^T \omega^+ = M^+ g - g}$ |
| Step 2. | Equation simplification:<br>$\boldsymbol{A' y = v'}$<br>subject to $(\boldsymbol{A_1^T} : v) = \begin{bmatrix} \boldsymbol{A'} : v' \\ \boldsymbol{A''} : v'' \end{bmatrix}$ |
| Step 3. | Optimum basis selection: |
| Step 4. | Deciding Vector:<br>If $\boldsymbol{d'^{(n)}} \neq 0$, go to step 6<br>Else, $\boldsymbol{\omega_1 = U_1 g} = \left[\omega_1^i, i \in \boldsymbol{S_1'}\right]^T$ |

# 5. THE WIRELESS CHANNEL: PROPAGATION AND CHANNEL MODELING PRINCIPLES

The performance of wireless communication systems is mainly affected by the wireless channel condition. As contrasting to the typically static and predictable characteristics of a wired channel, the wireless channel is rather dynamic and random, which makes an exact analysis of the wireless communication system often challenging. In the past years, optimization of the wireless communication system has become critical with the rapid growth of mobile communication systems and the emerging broadband mobile Internet access services. This means that the understanding of the wireless channels is an important step for developing high performance and bandwidth-efficient wireless communications systems.

## 5.1. Propagation Principles

In an ideal radio communication channel, the transmitted signal will travel through one direct path. This signal can be easily extracted in the receiver. However, in a real channel, the signal will be modified through its transmission in the channel. The signal on the receiver side will consist of a mix of attenuated, reflected, refracted, and diffracted copies of the original signal. In addition, the noise in the channel will be added to the signal and relative motion between the transmitter and the receiver will cause a shift in the carrier frequency (Doppler Effect). These effects on the signal are important to understand because the performance of a mobile radio system is dependent on the channel characteristics.

### 5.1.1. Propagation in Free Space and Antenna Gain

The free space propagation model is used to predict received signal strength when the transmitter and receiver have a clear, unobstructed line-of-sight path (LOS) between them. Satellite communication systems and microwave line-of-sight radio links typical-

ly undergo free space propagation. As with most large-scale radio wave propagation models, the free space model predicts that received power decays as a function of the Transmitter-Receiver (Tx-Rx) separation distance rose to some power (i.e., a power law function). The free space power received by a receiver antenna which is separated from a radiating transmitter antenna by a distance d, is given by the Friis free space equation [39],

$$P_R = \frac{P_T G_T}{4\pi d^2}\left(\frac{\lambda^2 G_R}{4\pi}\right) \tag{5.1}$$

where $P_t$, is the transmitted power, $P_r(d)$ is the received power which is a function of the Tx-Rx separation, $G_t$ is the transmitter antenna gain, $G_r$ is the receiver antenna gain, *d* is the Tx-Rx separation distance in meters.

From the above equation, we can write the propagation loss (path loss) as positive value after using the relationship (c=f $\lambda$) as follow,

$$\begin{aligned} L_F(dB) &= 10log_{10}\left(\frac{P_T}{P_R}\right) \\ &= -10log_{10}G_T - 10log_{10}G_R + 20log_{10}f \\ &\quad + 20log_{10}d + k \end{aligned} \tag{5.2}$$

where $k = 20log_{10}\left(\frac{4\pi}{3\times10^8}\right) = -147.56$

### 5.1.2. Reflection

Reflection is the physical phenomenon that occurs when a propagating electromagnetic wave face an object with very large dimensions compared to the wavelength, such as the surface of the earth and buildings. It forces the transmit signal power to be reflected back rather than being passed all the way along the path to the receiver. The amplitude and phase of the reflected signal is affected by the *reflection coefficient* at the point of reflection. The *reflection coefficient* itself is determined by material's conductivity, dielectric constant and angle, and it differs for vertical or horizontal polarization [39].

### 5.1.3. Diffraction

Diffraction refers to various phenomena that occur when the signal path between the transmitter and receiver is obstructed by a surface with sharp irregularities or small openings, which can be explained by the Huygens' Principle [39]. It appears as a bend-

ing of waves around the small obstacles and spreading out of waves past small openings. The secondary waves generated by diffraction are useful for establishing a path between the transmitter and receiver, even when a LOS path is not present [14].

### 5.1.4. Scattering

Scattering is the physical phenomenon that forces the radiation of an electromagnetic wave to deviate from a straight path by one or more local obstacles, with small dimensions compared to the wavelength. Those obstacles that induce scattering, such as foliage, street signs, and lamp posts, are referred to as the scatters. In other words, the propagation of a radio wave is a complicated and less predictable process that is governed by reflection, diffraction, and scattering, whose intensity varies with different environments at different instances [14].

### 5.1.5. Channel Fading

Most mobile communications happens in built up areas where the mobile antenna is well below the surrounding buildings with no LOS. The signal path therefore travels to the receiver by means of scattering, reflection and refraction. This usually results in the signal arriving through multiple paths simultaneously from different directions with different delays. The combination of the signal vectors at the receiver mobile equipment (ME) can be large or small depending on the phases of the components. A possible situation that can result in multipath fading is illustrated in figure 5.1 [39].

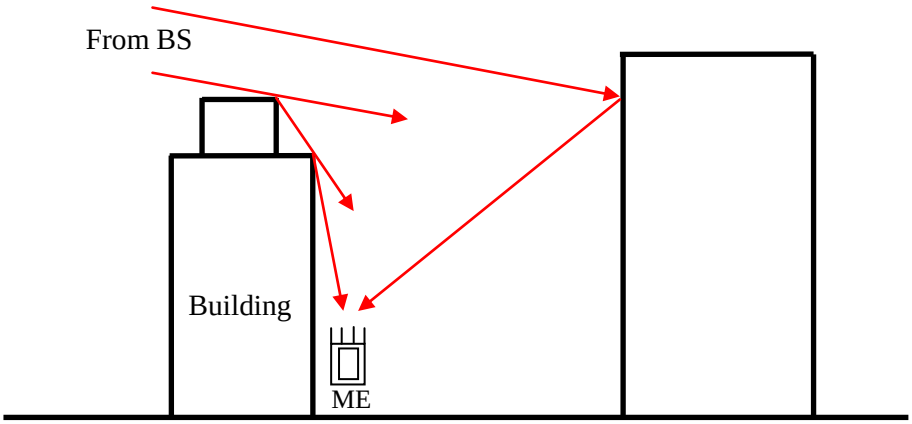


***Figure 5.1*** *Radio propagation in urban area*

Another type of fading is what's called *shadow fading*, which occur due to shadowing from obstacles that affect the propagation of the radio wave. First wireless communication channel models with fading conditions were modeled for HF (High Frequency, 3-30 MHz), UHF (Ultra HF, 300-3000 MHz), and SHF (Super HF, 3-30 GHz) bands in the 1950s and 1960s. At present, the most common wireless channel models have been established for 800 MHz to 2.5 GHz band by extensive channel measurements in the field.

For single antenna communication systems, referred to as Single Input Single Output (SISO), the ITU-R standard channel model was developed in [27] for certain frequencies. On the other hand, spatial channel models for a multi-antenna communication system, referred to as the MIMO (Multiple Input Multiple Output) system, have been recently developed by the various research and standardization bodies such as IEEE 802 [21][23], METRA Project [28], 3GPP/3GPP2 [3], and WINNER Projects [11][29], with the goal of high-speed wireless transmission and diversity gain [14].

The fading phenomenon can be mostly classified into two different types: small-scale fading and large-scale fading. Small-scale fading refers to fast variation of signal levels due to the constructive and destructive interference of multiple signal paths (multi-paths) when the ME moves short distances (usually at half wavelength distances). Depending on the relative level of a multipath, frequency selectivity of a channel is characterized (either frequency-selective or frequency flat) for small-scaling fading. Meanwhile, according to the time variation in the channel due to the relative speed between the transmitter and receiver (characterized by the Doppler spread), short-term fading can be classified as either fast fading or slow fading.

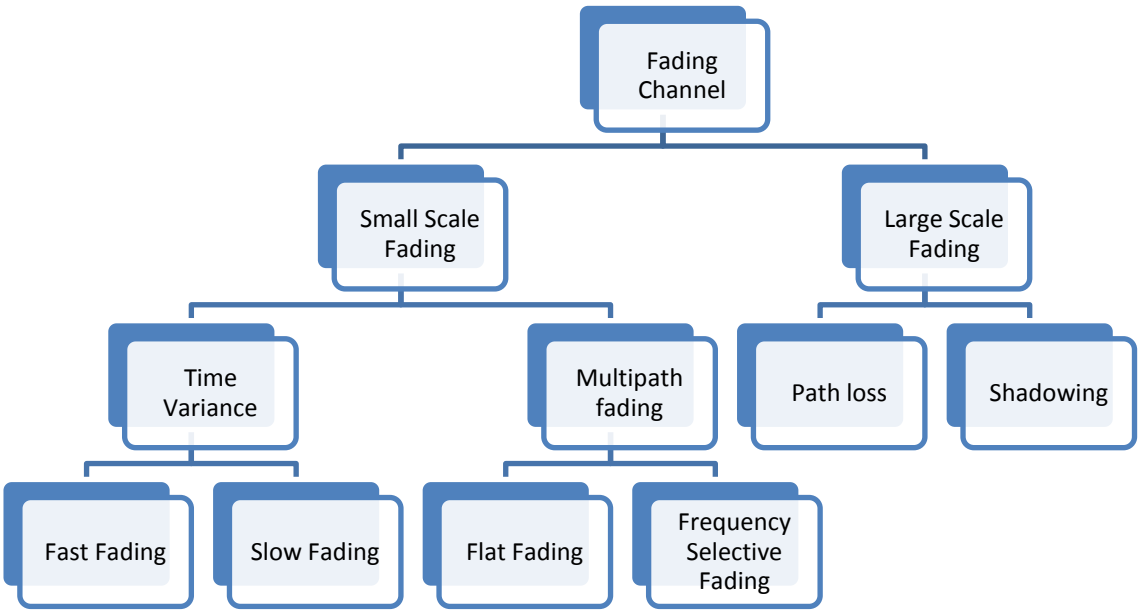


***Figure 5.2*** *Classification of the different fading channels*

On the other hand, large-scale fading occurs as the mobile moves through a large distance, for example, a distance of the order of cell size [46]. It is caused by path loss of signal as a function of distance and shadowing by large objects such as buildings, hills, etc. Shadowing is a slow fading process characterized by variation of median path loss between the transmitter and receiver in fixed positions. In other words, large-scale fading is characterized by average path loss and shadowing. Figure 5.2 classifies the types of fading channels [14].

## 5.2. Channel Modeling

An accurate channel model is a requirement for getting truthful and meaningful results when performing network planning or designing any communication system. Through a channel model, the different system parameters and ME/BS location is determined in order to study a new system design or simulate a network accurately before the need to build prototypes or perform broad measurements campaigns.

As discussed earlier, fading channels are classified into Large Scale and Small Scale fading channels. Channel models in practice include the effects of both models usually, although some studies can require modeling either large scale models or small scale models only. Channel models can also be classified to deterministic and stochastic models as will be briefly discussed next.

### 5.2.1. Deterministic Models

In the view of electromagnetic wave theory, the radio channel can be generally classified as deterministic channel model [33]. In deterministic channel modeling, a particular channel scenario is studied or modeled using different methods such as: electromagnetic simulation tools, ray-tracing or channel measurements. The deterministic channel will always produce the same results given the same starting parameters.

Deterministic channel models that utilize electromagnetic simulators are the most complex and demanding of computing power. The channel simulator tries to directly solve Maxwell's equations by using some numerical method like FEM (Finite Element Method) or MoM (Method of Moments), therefore offering accurate and detailed results of all the channel properties [15]. The use of this kind of simulators, or their hybrids, is generally limited in modeling small structures and locations, such as antenna arrays and antenna structures [44]. Together with its high demand for computing power, electromagnetic simulations also require very comprehensive information of the geometrical and electromagnetic properties of modeled objects, therefore increasing the complexity of this particular channel modeling method.

Ray tracing models are another type of deterministic channel modeling. If the wavelength is very small compared to the dimensions of the structures with which the waves interacts with in the environment, the propagating wave then can be modeled as rays [15]. Geometric optics theory operates with this kind of method. Channel propagation models based on geometric optics theory that uses rays are referred to as ray-tracing models. Ray-tracing models suffer from the high computational power needed in addition to the large amount of information about the environment. Mapping the environment in the horizontal domain is usually easy with the help of satellites images, but information about the vertical domain is usually inaccurate.

### 5.2.2. Stochastic Models

In stochastic channel modeling, also called statistical channel modeling, the channel behavior is modeled statistically based on large measurement campaigns. By using the data obtained through the measurements, the probability density function is studied and the channel impulse response is established [33]. Unlike deterministic modeling which

model a particular environment, stochastic modeling represents a certain class of environments or scenarios such as indoor hotspot, urban micro-cell, etc.

Stochastic modeling is suitable for system development and testing of different algorithms. This is because by running a single simulation for a class of environment, a large number of environments are statistically modeled, since the statistical elements are built into the model. This in turn gives another advantage, since we have a large number of environments modeled statistically into the model, there is no need for a large database for the simulator to run, and therefore less computing power is needed.

# 6. CA MIMO SYSTEM BER PERFORMANCE ANALYSIS

## 6.1. Simulation Overview

In order to acquire our results, our simulation go through two main steps with an intermediate step in-between as shown in figure 6.1. The first step is to generate the channel coefficients of the desired scenario (as channel impulse responses) for the simulation through a realistic channel model. Fast Fourier Transform (FFT) is then performed on the channel $H(t;\tau)$ to get the frequency representation. The last step is use the MHGOPA algorithm to find the optimal power allocation and calculate the BER.


***Figure 6.1*** *Simulation procedure*

For the purpose of generating the channel realizations $H(t;\tau)$ in our simulation, the ITU-R IMT-Advanced channel model was chosen. The model is geometry-based stochastic channel model in which the location of the scatterers is not specified, instead the directions of the rays are. This type of channel modeling was developed in WINNER projects (I and II) [11][29] and is based on the principles of 3GPP-3GPP2 Spatial Channel Model (SCM) [3] and the extension of it in SCM-Extension [12]. Table 6.1 and 6.2 provide features and numerical comparison between the different channel models [36;24;45].

The SCM channel model offers a bandwidth of 5 MHz only and its extension SCME, while having a max bandwidth of 100 MHz, is only an artificial extension from 5 MHz and without 100 MHz measurements. Carrier Aggregation (CA) is going to be implemented in LTE-Advanced with bandwidths ranging from 1.4-20 MHz, and a max-

imum 5 CCs. This will result in a system bandwidth of 100 MHz at max making the SCM channel model inadequate for our simulations.

***Table 6.1*** *Features Comparison*

| Feature | SCM | SCME | WINNER I | WINNER II | IMT-Adv |
|---|---|---|---|---|---|
| **Bandwidth > 20 MHz** | No | Yes | Yes | Yes | Yes |
| **Indoor Scenarios** | No | No | Yes | Yes | Yes |
| **Outdoor -to-Indoor Scenarios** | No | No | No | Yes | Yes |
| **AoA/AoD Elevation** | No | No | Yes | yes | No |
| **Time Evolution of Model Parameters** | No | Yes* | No | Yes | Yes |

* Continuous time evolution

***Table 6.2*** *Numerical Comparison*

| Parameter (unit) | SCM | SCME | WINNER I | WINNER II | IMT-Adv |
|---|---|---|---|---|---|
| **Max. Bandwidth (MHz)** | 5 | 100* | 100** | 100** | 100** |
| **Freq Range (GHz)** | 2 | 2 to 5 | 2 to 6 | 2 to 6 | 2 to 6 |
| **No. Of Scenarios** | 3 | 3 | 7 | 12 | 5 |
| **No. Of Clusters** | 6 | 6 | 4 to 24 | 4 to 20 | 10 to 20 |
| **No. Of mid-Paths per Cluster** | 1 | 3 to 4 | 1 | 1 to 3 | 1 to 3 |
| **No. Of sub-Paths per Cluster** | 20 | 20 | 10 | 20 | 20 |
| **No. Of Taps** | 6 | 18 to 24 | 4 to 24 | 4 to 24 | 14-24 |
| **BS Angle Spread (°)** | 5 to 19 | 4.7 to 18.2 | 3 to 38 | 2.5 to 53.7 | 6 to 42 |
| **ME Angle Spread** | 68 | 62.2 to 67.8 | 9.5 to 53 | 11.7 to 52.5 | 30-74 |
| **Delay Spread** | 170-650 | 231-841 | 1.6-313 | 16-630 | 20-365 |
| **Shadow Fading Standard Deviation** | 4 to 10 | 4 to 10 | 1.4 to 8 | 2 to 8 | 3 to 8 |

*Artificial extension from 5 MHz bandwidth

** Based on 100 MHz measurements

On the other hand, the IMT-ADV channel model was specifically tailored for the next generation systems 4G. The IMT-ADV channel model is actually achieved by the use of WINNER II channel model (which is an improvement to WINNER I), as will be explained in the next section.

### 6.1.1. WIM 2: IMT.EVAL Channel Model

The WIM2: IMT.EVAL is a modification of the WINNER Phase II Model (WIM) [30], from which we can generate radio channel realizations for both system and link level simulations. The scenarios supported for the channel model are: Indoor Hotspot (InH),

Urban Micro-cell (UMi), Urban Macro-cell (UMa), Suburban Macro-cell (SMa) and Rural Macro-cell (RMa). The channel model allows the user to define a large variety of parameters for the simulation, such as MIMO radio link parameters and antenna parameters. For a full list of input parameters and their description, refer to [31], *section 5.2.1 Input parameters*.

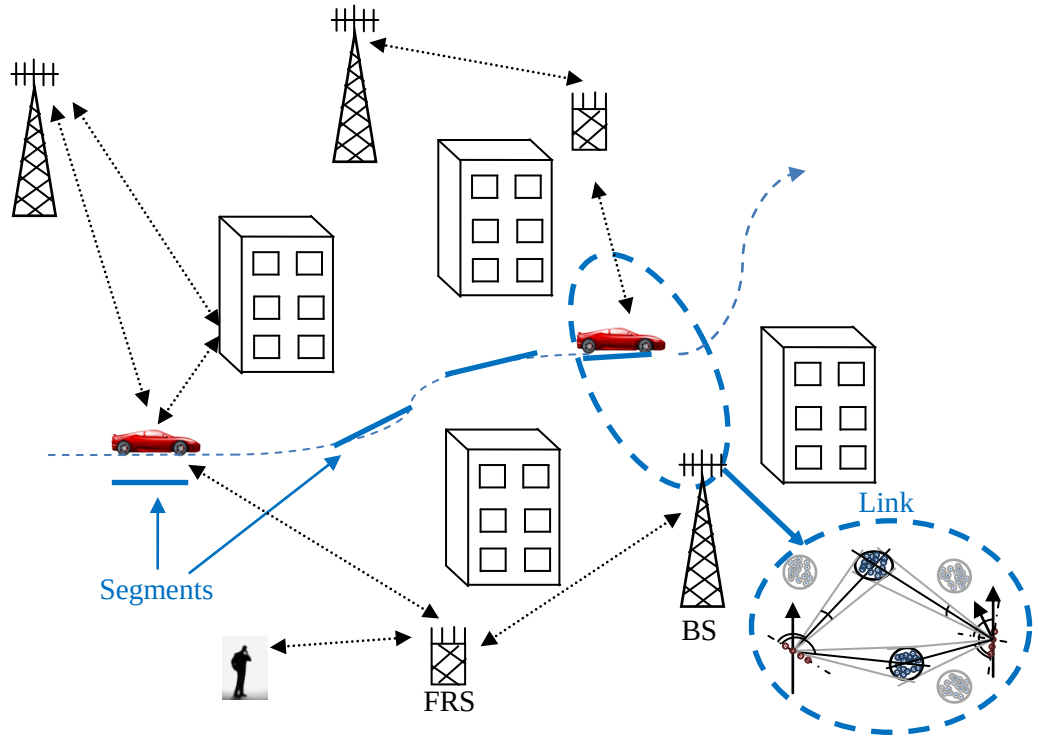


***Figure 6.2*** *System level approach with several segments (drops)*

The supported system level simulation can have multiple links simulated simultaneously with multiple BS's and ME's as shown in figure 6.2. The model simulates channel variation with time through *drops*, which are the time units in the simulation. The blue dash line, *segments*, indicates that the large scale parameters LS are fixed, while the dashed blue line indicates a single link simulation. Figure 6.3 shows the single link model with more details in which the parameters used are shown. The circle that includes many dots inside corresponds to a scattering region (single cluster) [29].

The channel parameters for different snapshots are determined stochastically based on statistical distribution that was extracted from different channel measurements. To generate the channel realizations, the simulator apply the geometrical principle by summing the contributions of different rays, each with its specific small scale (SS) parameters such as delay, power, AoD, and AoA [24].

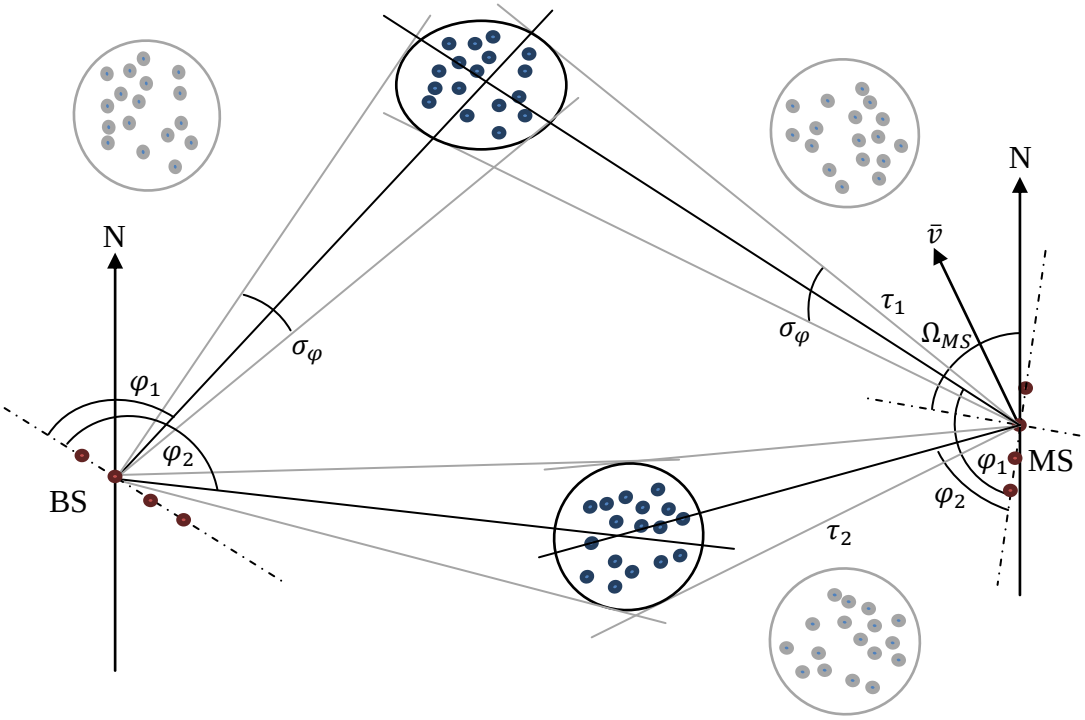


***Figure 6.3*** *Single Link*

The final time variant impulse response MIMO channel output is given by [24]:

$$\boldsymbol{H}(t;\tau) = \sum_{n=1}^{N} \boldsymbol{H}_n(t;\tau) \tag{6.1}$$

where *t* is time, $\tau$ is the delay, *N* is total number of paths, and *n* is the path index. $\boldsymbol{H}_n$ is composed of the antenna array response matrices $\boldsymbol{F}_{tx}$ and $\boldsymbol{F}_{rx}$ for the transmitter (Tx) and receiver (Rx) respectively, and the dual-polarized propagation channel response matrix $\boldsymbol{h}_n$, for cluster *n*, as follow:

$$\boldsymbol{H}_n(t;\tau) = \iint \boldsymbol{F}_{rx}(\varphi)\, \boldsymbol{h}_n(t;\tau,\phi,\varphi)\boldsymbol{F}_{tx}^{T}(\phi) d\phi d\varphi \tag{6.2}$$

## 6.2. Simulation Scenarios and Parameters

The simulations to generate the channel realizations were conducted for four scenarios that are summarized in table 6.3. Four frequency bands were generated with the channel model for each scenario. The bandwidth of each band is 100 MHz, with center frequencies located at 2.1 GHz, 2.6 GHz, 3.5 GHz, and 5.25 GHz. The MIMO configuration used is 4x4 with an antenna spacing of 0.5 $\lambda$ for the ME and 10 $\lambda$ for the BS antennas. Each scenario consisted of one BS and 4 ME's.

***Table 6.3*** *Simulated propagation scenarios*

| **Test Environment** | **Base Coverage urban** | | **Microcellular** | **Indoor** |
|---|---|---|---|---|
| **Deployment Scenario** | Urban macro-cell scenario | Suburban macro-cell scenario | Urban micro-cell scenario | Indoor hotspot Scenario |
| **Channel Model** | UMa (NLOS) | SMa (NLOS) | UMi (NLOS) | InH (NLOS) |
| **MIMO Configuration** | 4x4 | | | |
| **Channel Normalization** | Peak Value (Across the whole of H) | | | |
| **Number of Tx** | 4 | | | |
| **Antenna Spacing BS** | 10 $\lambda$ | | | |
| **Antenna Spacing Tx** | 0.5 $\lambda$ | | | |
| **Carrier Components** | 4 | | | |

The frequencies of the chosen subcarriers within the CCs for each scenario are presented in table 5.4, which shows Inter band non-contiguous CA used.

***Table 6.4*** *Frequencies used for CC1, CC2, CC3 and CC4*

| Scenario | UMa | SMa | UMi | InH |
|---|---|---|---|---|
| CC1 | 2.05 GHz | 2.55 GHz | 2.05 GHz | 2.05 GHz |
| CC2 | 2.58 GHz | 2.58 GHz | 2.57 GHz | 2.08 GHz |
| CC3 | 5.26 GHz | 5.26 GHz | 3.5 GHz | 2.108 GHz |
| CC4 | 5.25 GHz | 5.25 GHz | 5.25 GHz | 5.25 GHz |

## 6.3. Simulation Results

In this section we present the performance results obtained for the CA-MIMO radio link for the single Tx case using Matlab. The MHGOPA algorithm assumes a square 4-QAM modulation during the simulation. The following results are divided into four subsections. Each section presents the results for a different scenario environment, which is subsequently further studied in two cases.

The first case is to impose an equal power limit on all the CCs $P^C$, while the power constraint on each antenna is calculated by $P_i^A = \alpha_1 KP^C/N, \forall\, 1 \leq i \leq N$. We then evaluate the performance of the algorithm by varying antenna power constraint by $\alpha_1 = 1,2, \dots, N$. This will vary the antenna power constraint from a uniform power allocation per-antenna with $\alpha_1 = 1$, to a constraint-free antenna power allocation with $\alpha_1 = N$.

The second case is to grant a primary CC (PCC) power privilege $P_{pcc}^{C} = \alpha_2 N P^A/\alpha_1 K$ while limiting all the other secondary CC (SCC) by the same limit $P_{scc}^{C} =$ it $P_{scc}^{C} = P_{pcc}^{C}(K/\alpha_2 - 1)/(K-1)$. The power limit on the antennas will be the same $P^A$. The performance is then evaluated by varying $\alpha_2 = 1,2,\ldots,K$. The power constraint for the CCs will therefore vary from a uniform power allocation of $P^C = K$ with $\alpha_2 = 1$, to shutting down all the SCCs in favor of allocating all the power to the PCC at $\alpha_2 = K$.

In our simulation, we assume a transmission power matrix $P_j = I_N$, $j$ = 1,…,K. Since our simulation assumes a 4x4 MIMO system and 4 CCs, the total power, *in abstract value*, will be $P^T = 16$. The values of $P_i^A$, $P^C$, $P_{pcc}^{C}$, and $P_{scc}^{C}$ used during the simulations are presented in Table 6.5 and Table 6.6. For clarity sake, we provide the power constraint values in *mW* in parentheses next to the abstract value in the case of maximum TX power for LTE-Advanced UE (23dBm$\sim 200mW$) [5].

***Table 6.5*** *Simulation's power constraints by varying* $\alpha_1$

| $\alpha_1$ | $P^C$ | $P^A$ |
|---|---|---|
| 1 | 4(50 mW) | 4(50 mW) |
| 2 | 4(50 mW) | 8(100 mW) |
| 3 | 4(50 mW) | 12(150 mW) |
| 4 | 4(50 mW) | 16(200 mW) |

***Table 6.6*** *Simulation's power constraints by varying* $\alpha_2$

| $\alpha_2$ | $P^A$ | $P_{pcc}^{C}$ | $P_{scc}^{C}$ |
|---|---|---|---|
| 1 | 4(50 mW) | 4(50 mW) | 4(50 mW) |
| 2 | 4(50 mW) | 8(100 mW) | $2\frac{2}{3}$(33.3 mW) |
| 3 | 4(50 mW) | 12(150 mW) | $1\frac{1}{3}$(16.6 mW) |
| 4 | 4(50 mW) | 16(200 mW) | 0(0 mW) |

### 6.3.1. Indoor Hotspot Scenario

In this subsection, we investigate the performance in an indoor hotspot (InH) scenario where the ME is 20 m away from the BS with NLOS. The power, delay and angles parameters were taken from the CDL parameter table in Appendix I, Table A1.1. For the first case with $\alpha_1 = 1$, the MHGOPA algorithm shows a considerable improvement over the AVE (uniform power algorithm) power allocation. Figure 6.4 shows the com-

parison of the performance with uncoded BER, where MHGOPA outperform the AVE when the channel SNR is above ~8 dB.

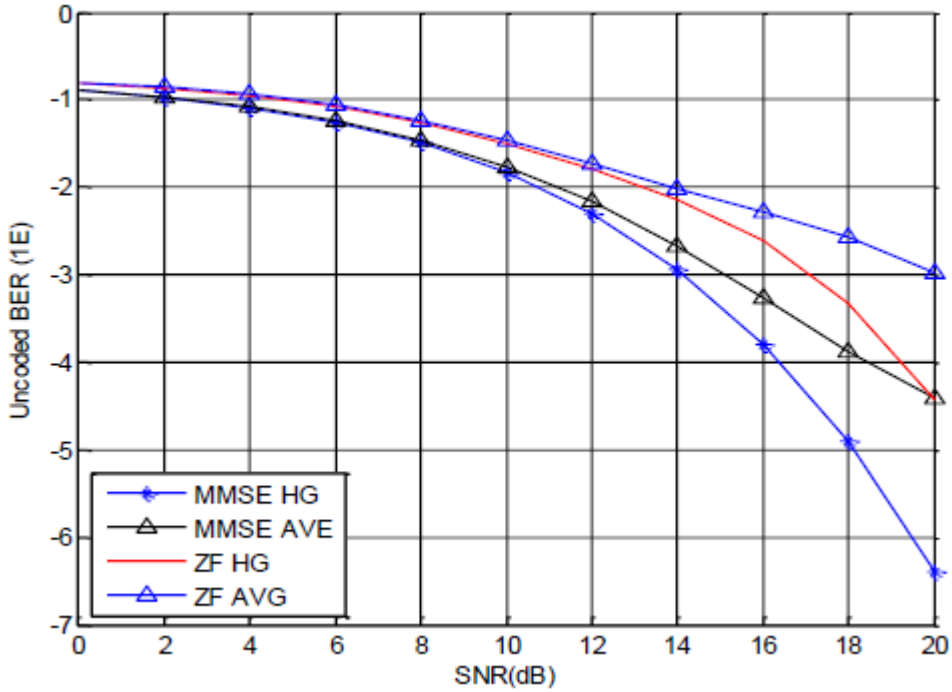


***Figure 6.4*** *InH: Average Uncoded BER with MMSE/ZF SIC receiver,* $\alpha_1$*=1*

When evaluating the performance for the MHGOPA with different antenna power constraints (by varying $\alpha_1$), the improvement in performance is barely visible. Figure 6.5 shows that setting $\alpha_1$=2 will barely increase the performance. Increasing $\alpha_1$ further will produce no improvement at all, which can be seen in the figure where the curves of $\alpha_1$=2, 3,4 are all on top of each other.

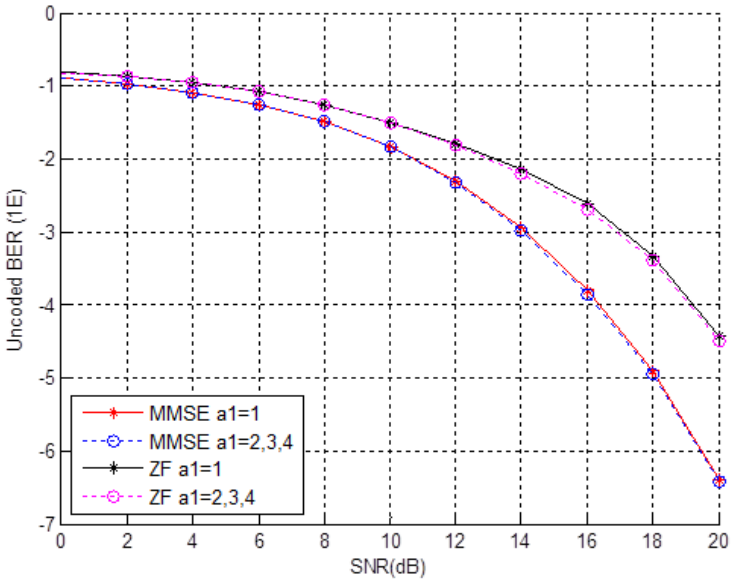

***Figure 6.5*** *InH: Average Uncoded BER with MMSE/ZF SIC receiver, varying* $\alpha_1$

Next we look at the behavior of the MHGOPA algorithm when we apply the concept of PCC and SCCs. Figure 6.6 show that the performance of the average Uncoded BER generally rapidly decreases the higher the privilege factor $\alpha_2$ while setting $\alpha_1 = 1$. Indeed the performance take a large hit when $\alpha_2$ is increased from 2 to 3. This observation is constant through the whole SNR range (0-20 dB). On the other hand, the performance of $\alpha_2 = 2$ overcomes, albeit slightly, the performance of $\alpha_2 = 1$ when the SNR is over 17 dB for the MMSE case, and 15 dB for the ZF case.

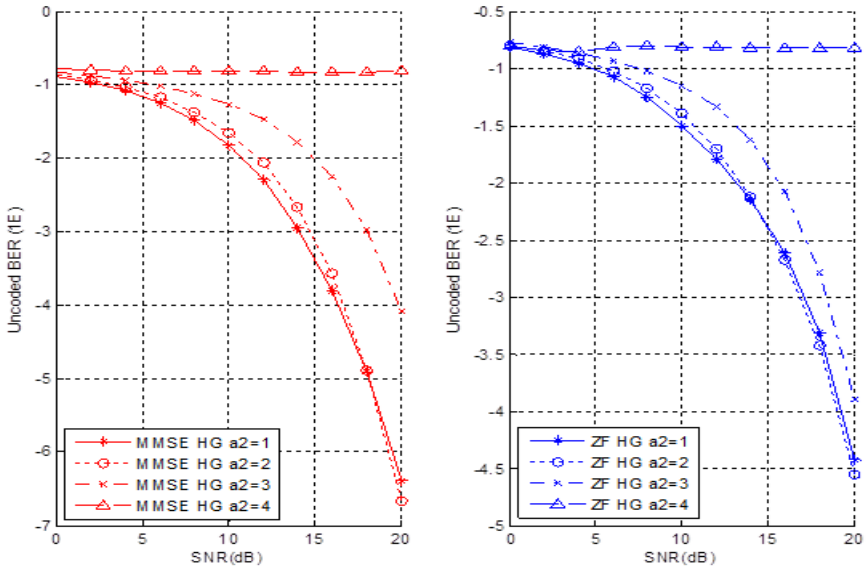


***Figure 6.6*** *InH: Average Uncoded BER with MMSE/ZF SIC receiver and PCC*

### 6.3.2. Urban Microcell Scenario

For the UMi scenario, we perform the same analysis to the MHGOPA algorithm we did with the InH. The ME here is 400 m away from the BS with NLOS. The power, delay and angles parameters were taken from the CDL parameter table in Appendix I, Table A1.2. For the first case with $\alpha_1 = 1$, the MHGOPA algorithm shows a good improvement over the AVE power allocation. Figure 6.7 shows the comparison of the performance with uncoded BER, where MHGOPA outperform the AVE when the channel SNR is above ~12 dB, unlike the InH scenario where the performance increase started at ~10 dB.

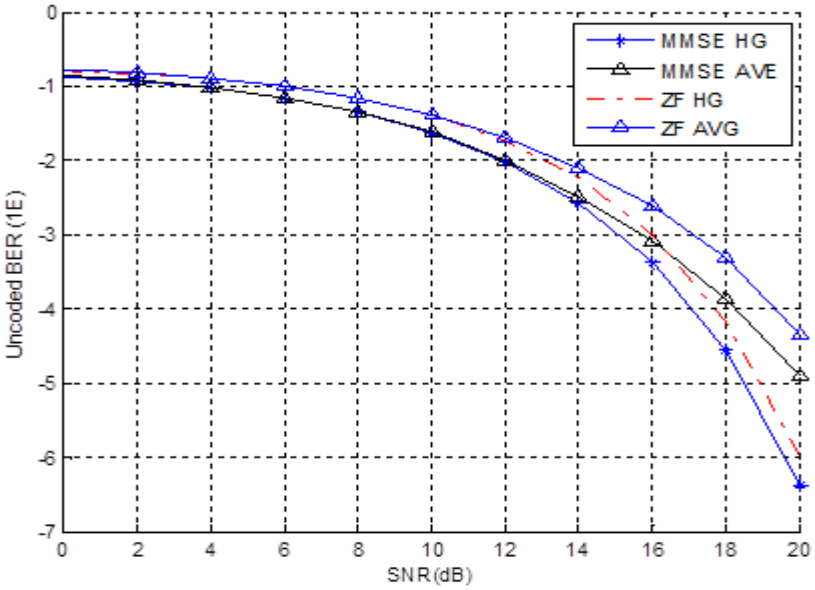


***Figure 6.7*** *UMi: Average Uncoded BER with MMSE/ZF SIC receiver,* $\alpha_1$*=1*

Next is evaluating the performance for the MHGOPA with different antenna power constraints (by varying $\alpha_1$). Unlike the InH scenario, the improvement in environment seems to be more noticeable. Similar to the InH environment, Figure 6.8 shows that increasing $\alpha_1$ above 2 will produce no improvement at all, as can be seen in the figure where the curves of $\alpha_1$=2, 3,4 are all on top of each other.

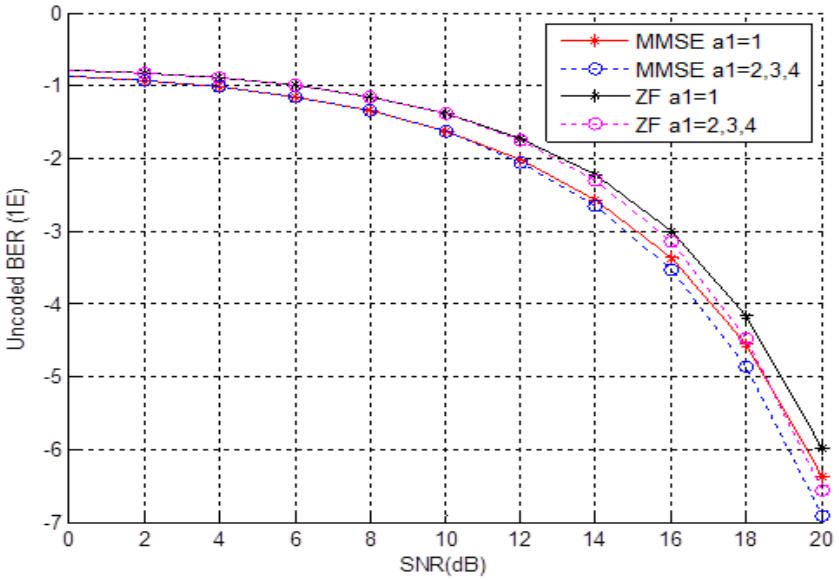


***Figure 6.8*** *UMi: Average Uncoded BER with MMSE/ZF SIC receiver, varying* $\alpha_1$

We finally then look at the behavior of the MHGOPA algorithm when we apply the concept of PCC and SCCs for the UMi environment. Figure 6.9 shows some differences to the InH environment. Most noticeable is that at no point of SNR does the privilege

factor $\alpha_2 = 2$ outperform $\alpha_2 = 1$. Also the difference in BER between the two is much larger.

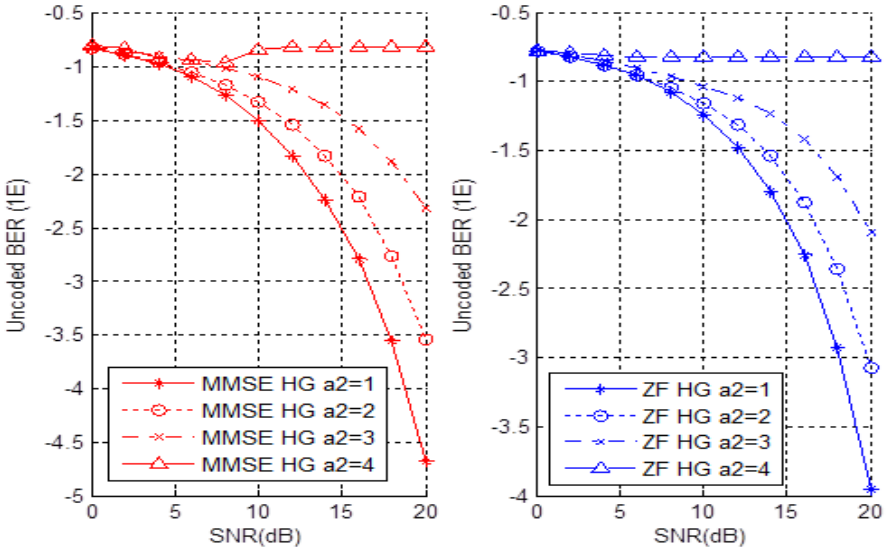


***Figure 6.9*** *UMi: Average Uncoded BER with MMSE/ZF SIC receiver and PCC*

### 6.3.3. Suburban Macrocell Scenario

The simulation results for the Suburban macro-cell (SMa) environment were similar to the InH results when varying the factor $\alpha_1 = 1$. The ME was simulated at 400 m distance from the BS with NLOS and the power, delay and angles parameters were taken from

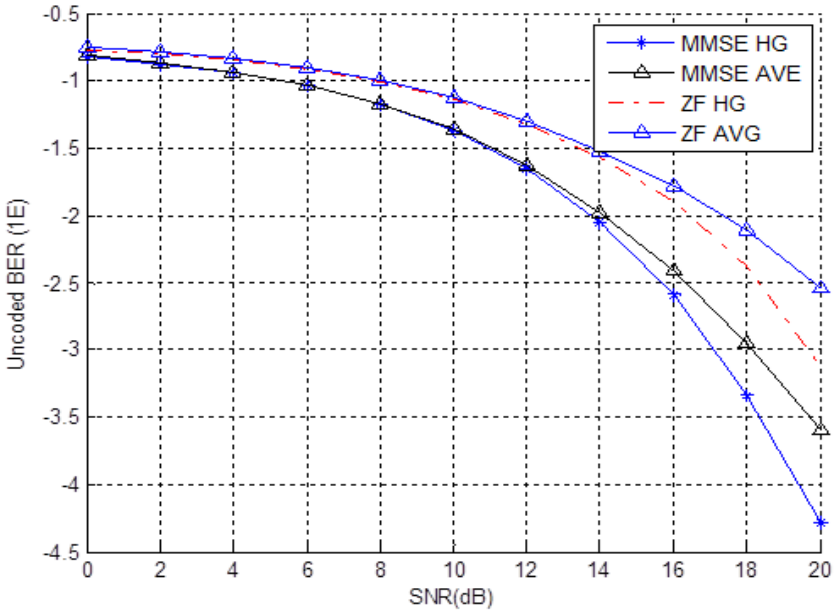


***Figure 6.10*** *SMa: Average Uncoded BER with MMSE/ZF SIC receiver,* $\alpha_1 = 1$

the CDL parameter table in Appendix I, Table A1.3. The MHGOPA expectedly outperform the AVE algorithm as shown in Figure 6.10 and shows a very small performance increase when $\alpha_1 > 1$ as can be seen in Figure 6.11

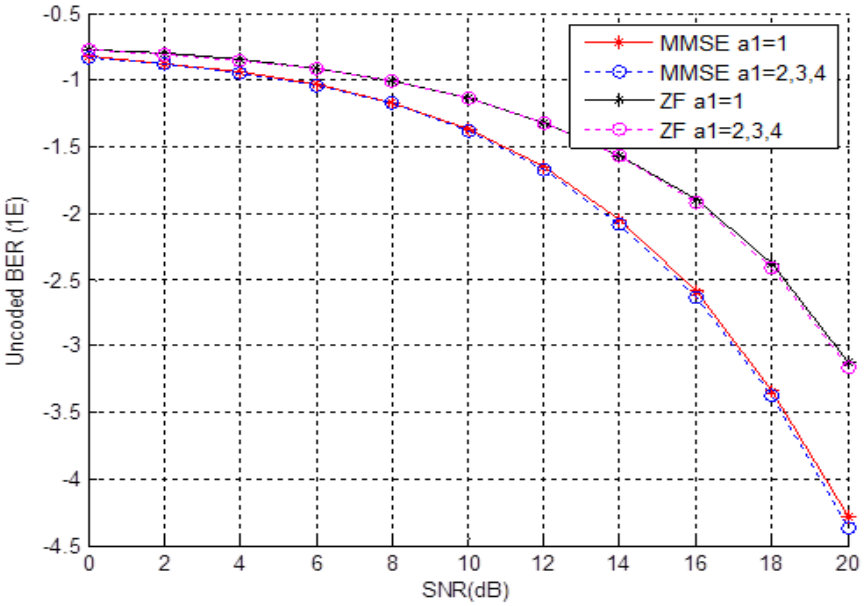


***Figure 6.11*** *SMa: Average Uncoded BER with MMSE/ZF SIC receiver, varying* $\alpha_1$

Figure 6.12 shows the MHGOPA algorithm when we apply the concept of PCC and SCCs for the SMa environment. Unlike the results for the $\alpha_1$ factor which were similar to the InH environment, the privilege factor $\alpha_2$ follows the same pattern of the UMi results. At no point of SNR does the privilege factor $\alpha_2 = 2$ outperform $\alpha_2 = 1$ and the difference in BER between the two is much larger than in InH. Note that $\alpha_2 = 4$ does not appear in figure 6.12. This is due to the algorithm getting into an infinite loop while trying to calculate the optimal values of the power matrix. It is safe to assume that the curve for $\alpha_2 = 4$ follows a similar pattern that appeared in both the InH and UMi environments.

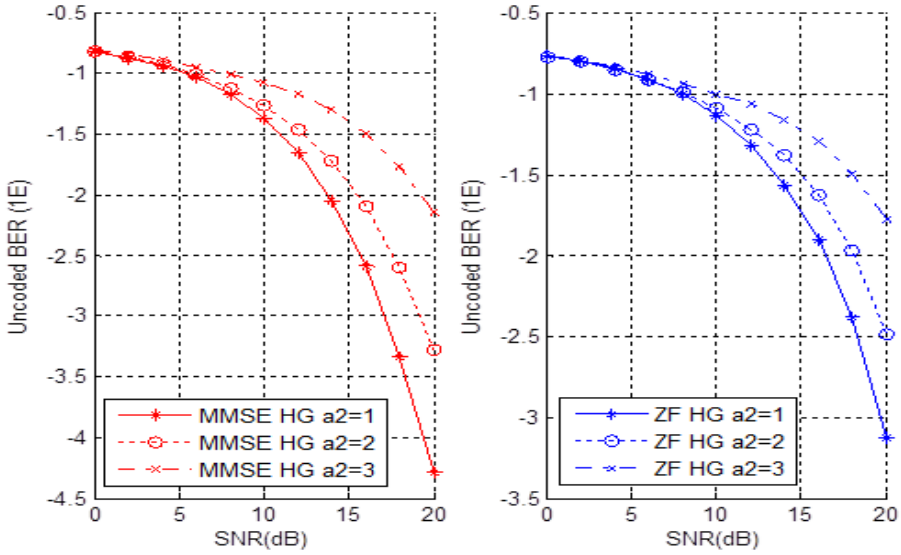


***Figure 6.12*** *SMa: Average Uncoded BER with MMSE/ZF SIC receiver and PCC*

### 6.3.4. Urban Macrocell Scenario

The last studied environment in this thesis is the Urban macro-cell (UMa) environment. During the simulation, the ME was positioned 400 m from the BS with NLOS. As with the previous scenarios, the parameters for the power, delays and angles were extracted from the CDL table in Appendix I, Table A1.4. Figure 6.13 show the UMa scenario results for the average Uncoded BER with $\alpha_1$=1. The MMSE MHGOPA algorithm performance shows the expected performance increase against the AVE algorithm. On the other hand, the ZF MHGOPA shows a very small performance increase against the AVE algorithm even at SNR value of 20 dB.

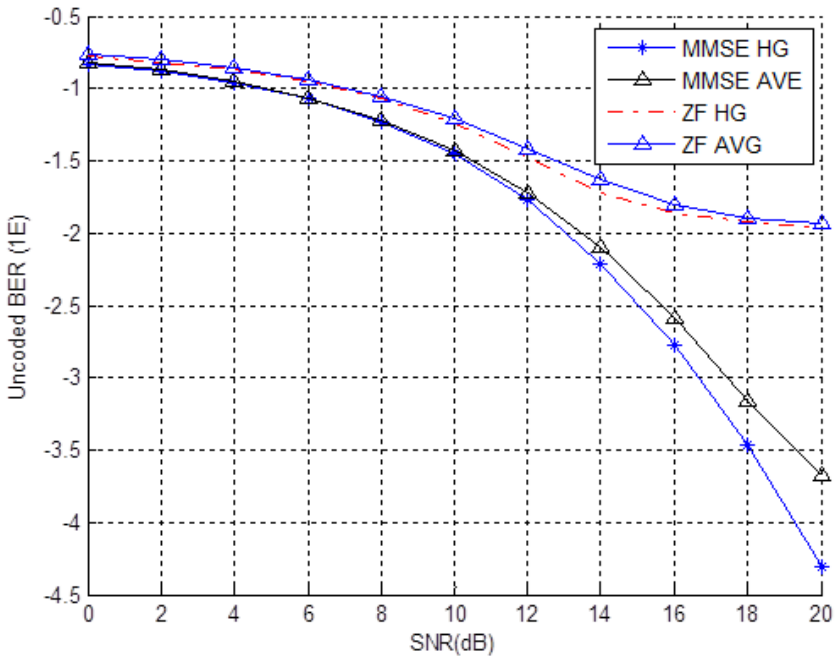


***Figure 6.13*** *UMa: Average Uncoded BER with MMSE/ZF SIC receiver,* $\alpha_1$*=1*

Figure 6.14 shows the MHGOPA with different antenna power constraints. Unlike the previous three environments, the four curves of $\alpha_1$=1,..,4 are all on top of each other with no differences in their performance. In figure 5.15, we can see that the implementation of the PCC function degrades the performance similar to the cases in UMi and SMa environments.

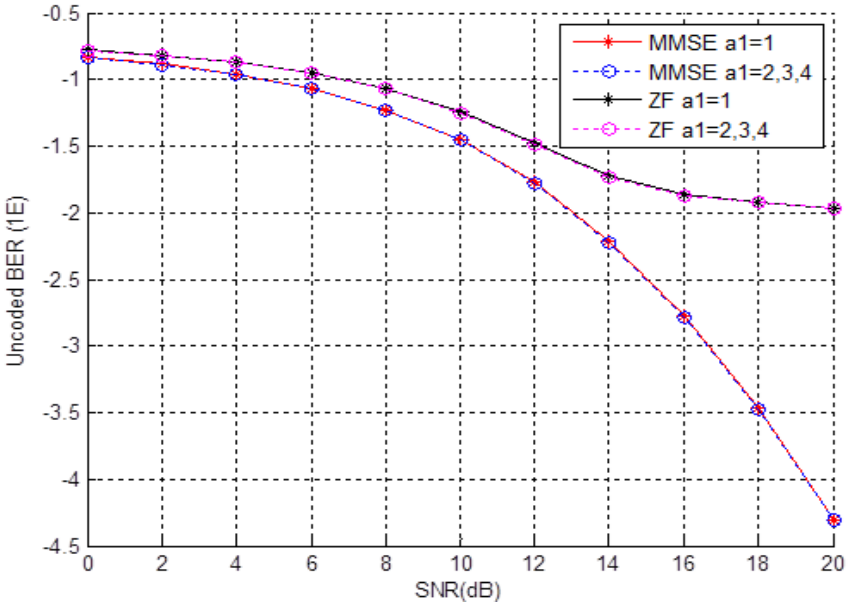


***Figure 6.14*** *UMa: Average Uncoded BER with MMSE/ZF SIC receiver, varying* $\alpha_1$

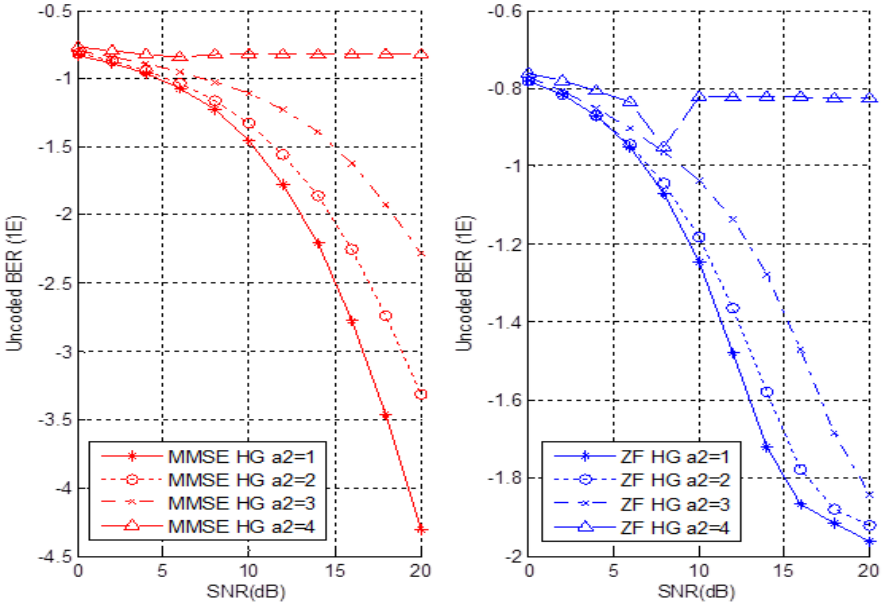


***Figure 6.15*** *UMa: Average Uncoded BER with MMSE/ZF SIC receiver and PCC*

# 7. DISCUSSION AND CONCLUSION

Carrier Aggregation promises a large increase in spectrum efficiency and with its ability to aggregate multiple carriers, it adds an extra constraint for power control (PC) policy in mobile systems. The MHGOPA algorithm studied in this thesis provides a PC policy method to optimize power allocation with multiple constraints on CCs, antennas and Tx. By testing the algorithm with different realistic channel environments (InH, UMa, UMi, and SMa) and different frequency bands in the 2-6 GHz range, we can have a better picture of the capabilities of the MHGOPA algorithm.

The results obtained in this thesis clearly show that the MHGOPA algorithm with its multiple power constraints, per-CC, antenna and Tx, outperform the baseline uniform power allocation in a CA-MIMO system. The improvement does not have a constant performance enhancement and it depends on the channel environment and conditions. We can observe this as follows:

1. The SNR point from which the MHGOPA algorithm starts to give a performance improvement differs from one scenario to another. While it starts at ~8 dB in the case of InH, in other environments it starts at ~12 dB.
2. By varying the factor $\alpha_1$ we can notice small improvements in scenarios InH, UMi, and SMa, but there was no improvement in the UMa results.
3. Varying $\alpha_2$ gives mixed results. In the InH scenario we can see that there was just a small degradation when changing the privilege factor $\alpha_2$ from 1 to 2, while the degradation was larger in the other scenarios. Not only that, but when the SNR is above a certain point (17 dB for MMSE and 15 dB for ZF), the performance actually becomes slightly better in the InH scenario.

The above three points show that a PC policy with the MHGOPA algorithm should take into consideration various variables and criteria. From point 1 we can clearly conclude that at SNR values below 8-12 dB (depending on the environment), the MHGOPA algorithm does not improve the performance and will only introduce further delay to the system to perform its lengthy calculations. In addition, the BS-ME will

need to constantly update the channel gain matrix *H* even though using the AVE power allocation will provide similar performance without the extra delay and data. Point 2 and 3 show that the performance's increase or decrease will vary depending on the different environments, and hence different channel characteristics and should be taken into consideration in the network planning.

Further study can be done towards finding the channel criteria to when it is beneficial to vary the CC and antenna constraints through the factors $\alpha_1$ and $\alpha_2$. Expanding the simulation to include multiple Tx's and BS's and investigating the effect of the algorithm time delay on the system performance is also worth exploring.

# *References:*


[1] 3GPP Rel-99 description, Overview of 3GPP Release 1999 V0.1.1 (2010-02), Available: http://www.3gpp.org/ftp/Information/WORK_PLAN/Description_Releases/

[2] 3GPP Release 9 description, Overview of 3GPP Release 9 V0.2.10 (2013-06), Available: http://www.3gpp.org/ftp/Information/WORK_PLAN/Description_Releases/

[3] 3GPP TR 25.996 V6.1.0, Spatial channel model for multiple input multiple output (MIMO) simulations, Sep. 2003.

[4] 3GPP TR 36.815 – V9.1.0, LTE-Advanced feasibility studies in RAN WG4, June 2010.

[5] 3GPP TS 36.101 –V10.10.0, User Equipment (UE) radio transmission and reception, 3GPP, March 2013.

[6] 3GPP TS 36.211 – V8.9.0, Physical Channels and Modulation, 3GPP, December 2009.

[7] 3GPP TS 36.212 – V8.8.0, Multiplexing and channel coding, 3GPP, December 2009.

[8] 3GPP TS 36.300 – V8.12.0, Overall description, 3GPP, March 2010.

[9] 802.11e Part 11: Wireless LAN Medium Access Control (MAC) and Physical Layer (PHY) Specifications Amendment 8: Medium Access Control (MAC) Quality of Service Enhancements, IEEE Std 802.11e-2005.

[10] S. M. Alamouti, “A Simple Diversity Technique for Wireless Communications,” IEEE Journal of select areas in communications, vol. 16, pp. 1451-1458, October 1998.

[11] D. S. Baum, H. El-Sallabi, T. Jämsä, J. Meinilä, P. Kyösti, X. Zhao, D. Laselva, J. P. Nuutinen, L. Hentilä, P. Vainikainen, J. Kivinen, L. Vuokko, P. Zetterberg, M. Bengtsson, K. Yu, N. Jaldén, T. Rautiainen, K. Kalliola, M. Milojevic, C. Schneider and J. Hansen, "Final Report on Link and System Level Channel Models", IST-WINNER D5.4, ver. 1.4, October 2005.

[12] D. S. Baum, J. Salo, G. D. Galdo, M. Milojevic, P. Kyösti and J. Hansen, “An interim channel model for beyond-3G systems,” Vehicular Technology Conference, 2005. VTC 2005-Spring. 2005 IEEE 61st, vol. 5, pp. 3132-3136, May 2005.

[13] L. H. Brandenburg and A. D. Wyner, “Capacity of the Gaussian Channel with Memory: The Multivariate Case,” Bell Syst. Tech. J., vol. 53, no. 5, pp. 745–778, May/June 1974.

[14] Y. S. Cho, J. Kim, W. Y. Yang and C. G. Kang, “MIMO-OFDM Wireless Communications with MATLAB,” John Wiley, Singapore, 2010.

[15] L. M. Correia, “Mobile Broadband Multimedia Networks: Techniques, Models and Tools for 4G,” Academic Press, 2006.

[16] Q. M. Cui, X. Q. Haung, B. Luo, X. F. Tao and J. Jiang, “Capacity analysis and optimal power allocation for coordinated transmission in MIMO-OFDM systems,” Science China Information Sciences, vol. 55, pp. 1372-1387, 2012.

[17] Q. M. Cui, P. C. Kang, X. Q. Huang, M. Valkama and J. Niemela, “Optimal power allocation for homogeneous and heterogeneous CA-MIMO systems,” Science China Information Sciences, vol. 56, Feb. 2013.

[18] R. Fleteher and C. M. Reeves, “Function minimization by conjugate gradient,” Computer Journal, vol. 7, pp. 149-154, 1964.

[19] Q. Gao, X. Zhang and J. Li, “Power control of V-BLAST system with per-antenna power constraints,” IEE Communications Letters, vol. 11, pp. 833-835, 2007.

[20] G. D. Golden, G. J. Foschini, R. A. Valenzuela and P. W. Wolniansky, “Detection algorithm and initial laboratory results using V-BLAST space–time communication architecture,” Electron. Lett., vol. 35, pp. 14–16, January 1999.

[21] K. V. S. Hari, K. P. Sheikh and C. Bushue, “Interim Channel Models for G2 MMDS Fixed Wireless Applications,” IEEE 802.16.3c-00/49r2, Nov. 15, 2000.

[22] H. Holma, A. Toskala, K. Ranta-aho and J. Pirskanen, “High-Speed Packet Access Evolution in 3GPP Release 7,” IEEE Communications Magazine, December 2007.

[23] IEEE 802.16 Broadband Wireless Access Working Group, Channel Models for Fixed Wireless Applications, IEEE 802.16.3c-01/29r4, July 2001.

[24] ITU-R M.2135-1, Guidelines for evaluation of radio interface technologies for IMT-Advanced, December 2009.

[25] ITU-R Rec. M.1645, Framework and Overall Objectives of the Further Development of IMT-2000 and Systems Beyond IMT-2000, 2003.

[26] ITU-R Rec. M.2134, Requirement Related to Technical Performance for IMT-Advanced Radio Interface, 2008.

[27] ITU-R Recommendation M.1225, Guidelines for evaluation of radio transmission technologies for IMT-2000, 1997.

[28] J. P. Kermoal, L. Schumacher and P. Mogensen, “Channel Characterisation,” IST-2000-30148 I-METRA D2, v1.1, Oct. 2002.

[29] P. Kyösti, J. Meinilä, L. Hentilä, X. Zhao, T. Jämsä, C. Schneider, M. Narandzić, M. Milojević, A. Hong, J. Ylitalo, V. M. Holappa, M. Alatossava, R. Bultitude, Y. Jong and T. Rautiainen, "WINNER II Channel Models", IST-WINNER D1.1.2 , ver. 1.1, Sept. 2007.

[30] P. Kyösti, J. Meinilä, L. Hentilä, X. Zhao, T. Jämsä, C. Schneider, M. Narandzić, M. Milojević, A. Hong, J. Ylitalo, V. M. Holappa, M. Alatossava, R. Bultitude, Y. Jong and T. Rautiainen, “WINNER II Interim Channel Models,” IST-WINNER II, D1.1.1 ver 1.2, February 2007.

[31] P. Kyösti, “Matlab SW documentation of WIM2 model,” v. 0.4, 2008.

[32] D. G. Luenberger, “Linear and Nonlinear Programming,” 3rd Edition, New York, 2009.

[33] X. Mao, J. Jin and J. Yang, “Wireless Channel Modeling Methods: Classification, Comparison and Application,” 5th International Conference on Computer Science & Education, China, August 2010.

[34] A. Nallanathan and L. Chang, “Eigenbeam-space division multiplexing for OFDM systems with optimum resource allocation,” IEEE Global Communications Conference, Dallas, pp. 2366-2370, 2004.

[35] S. H. Nam, O. Shin, K. B. Lee, “Transmit power allocation for a modified V-BLAST system,” IEEE Transactions on Communications, vol. 52, pp. 1074-1079, 2004.

[36] M. Narandzic, C. Schneider, R. Thoma, T. Jamsa, P. Kyosti and X. Zhao, “Comparison of SCM, SCME, and WINNER channel models,” Vehicular Technology Conference, 2007. VTC2007-Spring. IEEE 65th, pp. 413–417, Apr. 2007.

[37] Nokia Siemens Networks. (2010) [White Paper] Long Term HSPA Evolution: Mobile broadband evolution beyond 3GPP Release 10. Available:

http://www.nokiasiemensnetworks.com/sites/default/files/document/HSPA_evolution_white_paper_low_res_141220.pdf

[38] J. Oh, S. J. Kim and J. M. Cioffi, “Optimum power allocation and control for OFDM in multiple access channels,” IEEE Vehicular Technology Conference, Los Angeles, pp. 774-778, 2004.

[39] J. D. Parsons, “The Mobile Radio Propagation Channel,” 2nd Edition, John Wiley, Chichester, 2000.

[40] A. Paulraj, R. Nabar and D. Gore, “Introduction to Space-Time Wireless Communications,” Cambridge University Press, 2003.

[41] A. Paulraj and T. Kailath, US Patent No. 5345599 on Spatial Multiplexing, issued 1994.

[42] T. S. Rappaport, “Wireless Communications Principles and Practice,” 2nd Edition, Westford, March 2008.

[43] N. Reider and G. Fodor, “On opportunistic power control for MIMO-OFDM systems,” IEEE Global Communications Workshops, Miami, pp. 793-798, 2010.

[44] A. J. Sangster and H. Wang, "A hybrid FEM/MOM analysis for the scattering and radiating properties of a slot in slotted-waveguide array antennas," Second International Conference on Computation in Electromagnetics, pp. 386-389, 1994.

[45] S. Sesia, I. Toufik and M. Baker, “LTE – The UMTS Long Term Evolution: From Theory to Practice,” 2nd Edition, John Wiley & Sons, 2011.

[46] B. Sklar, “Digital Communications: Fundamentals and Applications,” 2nd Edition, Prentice Hall, 2002.

[47] N. Wang, S. D. Blostein, “Approximate minimum BER power allocation for MIMO spatial multiplexing systems,” IEEE Transactions Communications, vol. 55, pp. 180-187, 2007.

[48] H. Wang, C. Rosa, and K. Pedersen, "Performance of Uplink Carrier Aggregation in LTE-Advanced Systems," Vehicular Technology Conference Fall (VTC 2010-Fall), 2010 IEEE 72nd, pp. 1-5, September 2010.

[49] J. Wannstrom. (2012, May) LTE-Advanced. [Online]. Available: http://www.3gpp.org/LTE-Advanced

[50] Y. Xiao, "IEEE 802.11n: enhancements for higher throughput in wireless LANs," Wireless Communications, IEEE, vol. 12, no. 6, pp. 82-91, December 2005.

[51] W. Yu and T. Lan, “Transmitter optimization for the multi-antenna downlink with per-antenna power constraints,” IEEE Transactions on Signal Process, vol. 55, pp. 2646-2660, 2007.

[52] G. Yuan, X. Zhang and Y. Yang, “Carrier aggregation for LTE-advanced mobile communication systems,” IEEE communications Magazine, vol. 48, pp. 88-93, 2010.

# **APPENDIX** I

The following are the CDL models used in order to generate the channel realizations from the WIM2 IMT.ADV as given in [23].

***Table A1.1*** *Scenario InH NLOS CDL model, indoor hotspot*

| Cluster No. | Delay (ns) | Power (dB) | AoD (°) | AoA (°) | Ray Power (dB) | Cluster ASD =5 ° | Cluster ASA=11° | XPR=10 dB |
|---|---|---|---|---|---|---|---|---|
| 1 | 0 | -2,5 | -34 | 50 | -15,4 | | | |
| 2 | 15 | -1,9 | 34 | 50 | -15 | | | |
| 3 | 20 | -8,1 | 60 | -83 | -21,1 | | | |
| 4 | 25 | -1,8 | 24 | -30 | -14,8 | | | |
| 5 | 30 | 0 | -1 | -3 | -13 | | | |
| 6 | 40 | -2,3 | -31 | 44 | -15,4 | | | |
| 7 | 55 | -3,7 | 55 | -63 | -16,8 | | | |
| 8 | 60 | -8,4 | 69 | -105 | -21,4 | | | |
| 9 | 60 | -3,2 | 34 | -61 | -16,2 | | | |
| 10 | 70 | -9,7 | -73 | 110 | -22,7 | | | |
| 11 | 75 | -6,2 | -55 | -85 | -19,2 | | | |
| 12 | 75 | -8,9 | 56 | -85 | -21,9 | | | |
| 13 | 90 | -4 | -47 | 58 | -17 | | | |
| 14 | 150 | -14,1 | -84 | 121 | -27,1 | | | |
| 15 | 160 | -12,1 | 87 | -109 | -25,1 | | | |
| 16 | 170 | -10,6 | 71 | 108 | -23,6 | | | |
| 17 | 195 | -19,6 | -99 | 139 | -32,6 | | | |
| 18 | 205 | -16,8 | -99 | -137 | -29,8 | | | |
| 19 | 225 | -13,5 | 86 | 124 | -26,5 | | | |

***Table A1.2*** *Scenario UMi NLOS CDL model, urban micro-cell*

| Cluster No. | Delay (ns) | Power (dB) | AoD (°) | AoA (°) | Ray Pow-er(dB) | | | |
|---|---|---|---|---|---|---|---|---|
| 1 | 0 | -6,7 | 31 | -83 | -19,8 | Cluster ASD =10 ° | Cluster ASA=22° | XPR=8 dB |
| 2 | 10 15 10 | -4.9 -7.1 -8.9 | 10 | 54 | -14,7 | | | |
| 3 | 20 | -1,9 | 26 | 37 | -14,9 | | | |
| 4 | 35 | -6,3 | -27 | 96 | -19,3 | | | |
| 5 | 40 45 50 | -3 -5.2 -7 | -3 | 3 | -13 | | | |
| 6 | 55 | -7,5 | -29 | -86 | -20,5 | | | |
| 7 | 55 | -6,4 | -33 | 84 | -19,4 | | | |
| 8 | 200 | -10,8 | 37 | -112 | -23,9 | | | |
| 9 | 205 | -5,2 | -29 | -78 | -18,2 | | | |
| 10 | 250 | -4,9 | 27 | 65 | -17,9 | | | |
| 11 | 330 | -9,2 | -35 | -88 | -22,3 | | | |
| 12 | 440 | -15,5 | -48 | -130 | -28,5 | | | |
| 13 | 440 | -16,7 | -50 | 153 | -29,7 | | | |
| 14 | 515 | -12,4 | -44 | 106 | -25,5 | | | |
| 15 | 530 | -16,9 | 46 | 147 | -29,9 | | | |
| 16 | 580 | -12,7 | -45 | 118 | -25,7 | | | |
| 17 | 590 | -23,5 | -59 | -178 | -36,5 | | | |
| 18 | 625 | -22,1 | 60 | -163 | -35,1 | | | |
| 19 | 730 | -23,6 | 56 | 163 | -36,6 | | | |

***Table A1.3*** *Scenario SMa NLOS CDL model, suburban macro-cell*

| Cluster No. | Delay (ns) | Power (dB) | AoD (°) | AoA (°) | Ray power (dB) | | | |
|---|---|---|---|---|---|---|---|---|
| 1 | 0 5 10 | -3 -5.2 -7 | 0 | 0 | -13 | Cluster ASD=2° | Cluster ASA=10° | XPR=4dB |
| 2 | 25 | -7.5 | 13 | -71 | -20.5 | | | |
| 3 | 35 | -10.5 | -15 | -84 | -23.5 | | | |
| 4 | 35 | -3.2 | -8 | 46 | -16.2 | | | |
| 5 | 45 50 55 | -6.1 -8.3 -10.1 | 12 | -66 | -16.1 | | | |
| 6 | 65 | -14 | -17 | -97 | -27 | | | |
| 7 | 65 | -6.4 | 12 | -66 | -19.4 | | | |
| 8 | 75 | -3.1 | -8 | -46 | -16.1 | | | |
| 9 | 145 | -4.6 | -10 | -56 | -17.6 | | | |
| 10 | 160 | -8 | -13 | 73 | -21 | | | |
| 11 | 195 | -7.2 | 12 | 70 | -20.2 | | | |
| 12 | 200 | -3.1 | 8 | -46 | -16.1 | | | |
| 13 | 205 | -9.5 | 14 | -80 | -22.5 | | | |
| 14 | 770 | -22.4 | 22 | 123 | -35.4 | | | |

***Table A1.4*** *Scenario UMa NLOS CDL model, urban macro-cell*

| Cluster No. | Delay (ns) | Power (dB) | AoD (°) | AoA (°) | Ray Power(dB) | Cluster ASD =2 ° | Cluster ASA=15° | XPR=7 dB |
|---|---|---|---|---|---|---|---|---|
| 1 | 0 5 10 | -3.5 -5.7 -7.5 | 6 | 29 | -13.5 | | | |
| 2 | 5 | -9.2 | 44 | -98 | -22.2 | | | |
| 3 | 20 25 30 | -3 -5.2 -7 | 2 | 8 | -13 | | | |
| 4 | 45 | -7.8 | -34 | -114 | -20.8 | | | |
| 5 | 265 | -3.7 | 26 | 70 | -16.7 | | | |
| 6 | 290 | -8.6 | -41 | 107 | -21.6 | | | |
| 7 | 325 | -2.5 | -17 | 59 | -15.5 | | | |
| 8 | 340 | -7.3 | -33 | -103 | -20.3 | | | |
| 9 | 355 | -3.8 | 24 | 73 | -16.8 | | | |
| 10 | 440 | -6.9 | -34 | -111 | -19.9 | | | |
| 11 | 555 | -8.9 | -38 | -112 | -21.9 | | | |
| 12 | 645 | -9 | 44 | 122 | -22 | | | |
| 13 | 970 | -9.8 | 53 | 129 | -22.8 | | | |
| 14 | 1015 | -15 | 54 | 153 | -28 | | | |
| 15 | 1220 | -13.4 | 53 | -145 | -26.4 | | | |
| 16 | 1395 | -14.9 | 52 | -157 | -27.9 | | | |
| 17 | 1540 | -16.7 | 57 | -178 | -29.7 | | | |
| 18 | 1750 | -11.2 | 53 | -114 | -24.2 | | | |
| 19 | 1870 | -18.2 | -54 | -160 | -31.2 | | | |
| 20 | 1885 | -17.8 | -60 | -175 | -30.8 | | | |